Applied Catalysis A, General 632 (2022) 118511

Contents lists available at ScienceDirect

Applied Catalysis A, General

journal homepage: www.elsevier.com/locate/apcata

# Novel Ce-modified cobalt catalysts supported over α-$Al_2O_3$ open cell foams for lean methane oxidation

Andoni Choya [a], Sylwia Gudyka [b], Beatriz de Rivas [a], Jose Ignacio Gutiérrez-Ortiz [a], Andrzej Kotarba [b], Rubén López-Fonseca [a,*]

[a] Chemical Technologies for Environmental Sustainability Group, Department of Chemical Engineering, Faculty of Science and Technology, University of The Basque Country UPV/EHU, Barrio Sarriena s/n, Leioa Bizkaia E-48940, Spain
[b] Materials and Surface Chemistry Group, Faculty of Chemistry, Jagiellonian University, Gronostajowa 2, Krakow P-30-387, Poland

ARTICLE INFO

*Keywords:*
Lean methane oxidation
Natural gas vehicles
Ce-promoted cobalt catalysts
Open-cell ceramic foams
Solution combustion synthesis

ABSTRACT

A series of $CeO_2$-modified $Co_3O_4$ catalysts supported over α-$Al_2O_3$ foams was prepared by solution combustion synthesis and examined for the lean methane oxidation. Two different fuels were used namely, urea and glycine, with varying fuel/oxidiser (Φ) ratio. The catalysts were characterised by SEM-EDX, STEM-HAADF coupled to EDX mapping, ICP-AES, WDXRF, $N_2$ physisorption, XRD, HRTEM, Raman spectroscopy, XPS, $H_2$-TPR and $CH_4$-TPRe, and their activity in the abatement of methane was analysed under realistic conditions. The use of glycine produced catalysts with significantly better morphological and structural properties. Likewise, a favoured insertion of cerium cations into the $Co_3O_4$ spinel lattice was observed, which caused a significant distortion of the spinel structure, thereby leading to a higher amount of mobile oxygen species capable of oxidising methane. These beneficial structural alterations were more pronounced with higher Φ ratios.

## 1. Introduction

Use of natural gas as an alternative vehicle fuel to gasoline and diesel is growing worldwide due to the fact that it produces significantly less emissions of greenhouse gases, while being cheaper and safer [1]. However, more technological efforts are required to increase the efficiency of catalytic converters to reduce the trace amounts of unburned methane in the exhaust gases due to its notable environmental impact. It is widely accepted that palladium catalysts are the most active candidates for methane oxidation [2]. Alternatively, the main cheaper noble metal-free substitutes are cobalt-based catalysts, namely those based on cobalt oxides such as the spinel-type $Co_3O_4$ due to the remarkable mobility of its oxygen species [3,4]. This material has already been extensively investigated for numerous applications such as CO oxidation [5,6], $N_2O$ abatement [7,8] or oxidation of VOCs [9] and soot [10].

Most studies on the design of efficient catalysts are referred to powdered or pelleted systems although the real implementation in natural gas vehicles would need a more suitable catalyst geometry that minimises gas flow resistance and facilitates intensification of the catalytic process of lean methane oxidation. Monolith catalysts are usually the preferred option due to their good thermal and mechanical resistance [11,12]. However, an alternative solution has lately appeared in the form of open cell foams made of ceramic or metallic materials, which are characterised by a cellular structure with interconnected and often non-ordered pores with a large volume [13]. Typically, only 5–25% of the total volume of the foam is the base material. The alleged advantage of this type of structured substrates when compared with more conventional monoliths lies on their high surface/volume ratio and random disposition of the void volume, which can aid in the mass and heat transfer between the gas and the solid phase and allow rector operation at relatively high flow rates [14]. The use of foam-supported catalysts is currently focused on both pollution abatement processes (catalytic converters) [15–17] or conventional catalytic processes such as methane reforming or $CO_2$ methanation [18–20].

The incorporation of a powdered catalyst onto a structured support can be mainly carried out by two methodologies. The most commonly applied procedure on an industrial scale is to prepare a washcoating slurry with the powdered catalyst and a fluid phase such as water or a water/glycerine mixture. The structured support is then dipped into the slurry until it is thoroughly coated. Next, the samples is dried and calcined to stabilise the catalytic phase material [21]. A second approach involves applying impregnation-based routes to deposit the

* Corresponding author.
*E-mail address:* ruben.lopez@ehu.eus (R. López-Fonseca).

https://doi.org/10.1016/j.apcata.2022.118511
Received 17 November 2021; Received in revised form 7 January 2022; Accepted 22 January 2022
Available online 25 January 2022

catalyst formulation directly onto the surface of the structured support. The most frequently used methods in this case are wet impregnation (often in the presence of some surfactants) and solution combustion synthesis (SCS) [22,23]. Essentially, SCS is understood as a self-sustained reaction of metal nitrates and an organic fuel with varying chemical nature, which induces a high-temperature reaction between fuel and oxygen-containing species derived from the decomposition of the nitrates. This methodology entails a series of advantages. For instance, in addition to avoiding the intermediate and time-consuming steps of washcoating, the SCS route usually leads to well crystallised nanosized clusters after thermal stabilisation [24,25]. In this sense, when evaluating cobalt catalysts supported on α-$Al_2O_3$ coated monoliths for $N_2O$ decomposition, Wójcik et al. [26] evidenced a better catalytic performance of deposited $Co_3O_4$ by SCS with respect to conventional impregnation. The key operational parameters of the SCS route are basically the selection of the fuel and the appropriate fuel-to-oxidiser (metallic nitrates) ratio, which is typically denoted as Φ. These two factors strongly influence the mechanism of the combustion process and, in turn, the morphological properties of the active phase.

In this work attention was paid to analysing the use of two different fuels, namely urea and glycine, since these are cheap and readily available commercially, while the Φ ratio was varied from 0.25 to 1.0, which corresponded to 25–100% stoichiometric amount of fuel, respectively. An α-$Al_2O_3$ open cell foam was chosen due to its stability at relatively high temperatures and chemical inertness. Based on our previous study [27] dealing with the design of α-$Al_2O_3$ supported Co-Ce powdered catalysts for lean methane oxidation, the selected active phase was $Co_3O_4$ with a loading of 10%wt modified with controlled amounts of cerium as a promoter (Ce/Co molar ratio of 0.05). Both active phases were simultaneously incorporated in the same SCS step. The set of structured catalysts prepared by solid combustion synthesis was examined in the oxidation of lean methane under realistic conditions (relatively high space velocity and simultaneous presence of notable amounts of $H_2O$ and $CO_2$ in the flue gas) for a prolonged reaction time interval (285 h at 550 ºC). Catalytic results were kinetically analysed in terms of the reaction rate normalised to the $Co_3O_4$ mass for a selected reaction temperature (400 ºC).

## 2. Experimental

### 2.1. Synthesis of the structured catalysts

An α-$Al_2O_3$-based open cell foam (Lanik, s.r.o., 45 ppi, length = 30 mm and diameter = 8 mm) was selected as the structured support. Table S1, Supplementary Material, summarises the main geometric properties of the foam substrate. The average strut thickness (0.42 mm) and pore size (1 mm) were estimated from various SEM micrographs similar to those shown in Fig. S1, Supplementary Material. The calculated porosity or voidage was 0.78. The followed procedure for estimating this physical parameter, which depends on the average strut thickness and the average pore diameter, is detailed in the Supplementary Material. On the other hand, it should be noted that, in addition to alumina, appreciable amounts of silica (18%wt.) and magnesia (1% wt.) were present as determined by WDXRF.

The foam catalysts were synthesised by solid combustion synthesis using urea and glycine as fuels. Samples were prepared with varying fuel/oxidiser ratio (Φ), namely 0.25, 0.50, 0.75 and 1.00. The selected cobalt loading was 10%wt.$Co_3O_4$ with a Ce/Co molar ratio of 0.05 that was equivalent to a 1 wt.$CeO_2$%. The SCS impregnation gel was an aqueous solution of cobalt nitrate hexahydrate ($Co(NO_3)_2.6\,H_2O$) 0.4 M and cerium nitrate hexahydrate ($Ce(NO_3)_3.6\,H_2O$) 0.02 M in which adjusted amounts of the used fuel for the various selected Φ ratios were dissolved. In all cases, the open cell foams were dipped vertically into 25 ml of the corresponding impregnation solution for 5 min. Then, the excess was removed with compressed air. The impregnated foam was subsequently placed in an oven at 250 °C for 20 min with the aim of inducing the SCS reaction. This coating procedure was repeated several times to reach the desired cobalt and cerium concentration. After the last impregnation step, the coated foams were calcined at 600 °C for 4 h to produce the final catalysts. The samples were labelled as F(U) and F(G) when using urea and glycine, respectively.

The chemical reactions that ideally occur between the metal nitrates and the selected fuels during the combustion step as a function of the Φ ratio are the following:

$$Co(NO_3)_2 + \frac{14}{9}\Phi CO(NH_2)_2 + \frac{7}{3}(\Phi-1)O_2 \rightarrow \frac{1}{3}Co_3O_4 + \frac{14}{9}\Phi CO_2 + \frac{28}{9}\Phi H_2O + \left(\frac{14}{9}\Phi + 1\right)N_2$$

$$Ce(NO_3)_3 + \frac{7}{3}\Phi CO(NH_2)_2 + \frac{7}{2}(\Phi-1)O_2 \rightarrow CeO_2 + \frac{7}{3}\Phi CO_2 + \frac{14}{3}\Phi H_2O + \left(\frac{14}{6}\Phi + \frac{3}{2}\right)N_2$$

$$Co(NO_3)_2 + \frac{28}{27}\Phi C_2H_5NO_2 + \frac{7}{3}(\Phi-1)O_2 \rightarrow \frac{1}{3}Co_3O_4 + \frac{56}{27}\Phi CO_2 + \frac{70}{27}\Phi H_2O + \left(\frac{14}{27}\Phi + 1\right)N_2$$

$$Ce(NO_3)_3 + \frac{14}{9}\Phi C_2H_5NO_2 + \frac{7}{2}(\Phi-1)O_2 \rightarrow CeO_2 + \frac{28}{9}\Phi CO_2 + \frac{35}{9}\Phi H_2O + \left(\frac{7}{9}\Phi + \frac{3}{2}\right)N_2$$

Thus, when Φ = 0 the reaction corresponds to the simple thermal decomposition of the metallic (cobalt or cerium) nitrate. If Φ = 1, the corresponding stoichiometric redox reaction is then made explicit. Taking into account that the required $Co_3O_4$ and $CeO_2$ concentrations were 10%wt and 1%wt., respectively, the extent of the redox reactions involving cobalt nitrate was comparatively more noticeable since a larger amount of this salt was used in the synthesis.

### 2.2. Characterisation techniques

The foam catalysts were characterised by a wide number of analytical techniques including scanning electron microscopy (SEM) coupled to energy dispersive X-ray spectroscopy (EDX), scanning transmission electron microscopy - high angle annular dark field (STEM-HAADF) coupled to EDX mapping, inductively coupled plasma atomic emission spectroscopy (ICP-AES), wavelength dispersive X-ray fluorescence (WDXRF), $N_2$ physisorption, X-Ray diffraction (XRD), high resolution transmission electron microscopy (HRTEM), Raman spectroscopy, X-Ray photoelectron spectroscopy (XPS), temperature-programmed reduction with hydrogen ($H_2$-TPR) and temperature programmed reaction with methane ($CH_4$-TPRe). Except for SEM-EDX, the structured catalysts were crushed and milled to a fine powder before analysis. Although the experimental details are included elsewhere [28,29], some relevant details on the characterisation details are given below.

Scanning Electron Microscopy images were obtained in a JEOL JSM-7000 F Schottky-type field emission microscope operated at 10 kV. The electronic microscope was equipped with a INCA X-sight Si(Li) series pentaFET EDX detector to allow for elemental analysis of the observed surfaces. On the other hand, High-Resolution Transmission Electron Microscopy and Scanning Transmission Electron Microscopy images were obtained with a in a Cs-image-corrected Titan (Thermofisher Scientific) at a working voltage of 300 kV with a 2k x 2k Ultrascan CCD camera (Gatan) positioned before the filter for TEM imaging (energy resolution of 0.7 eV). The microscope was equipped with a CCD camera (Gatan), a HAADF detector (Fischione) and an Ultim Max detector (Oxford Instruments) that allowed for EDX elemental mapping.

The elemental composition of the synthesised catalysts was

determined by ICP-AES, using a Thermo Elemental Iris Intrepid apparatus, and WDXRF with a PANalytical AXIOS sequential spectrometer. The textural properties, in terms of specific surface area (BET method) and pore volume (BJH method), were determined by nitrogen physisorption at − 196 °C in a Micromeritics TriStar II apparatus. Before the analysis, outgassing of the samples was carried out on a Micromeritics SmartPrep apparatus at 300 ºC for 10 h with a $N_2$ flow.

XRD analysis were carried out using Cu Kα radiation (λ = 1.5406 Å) on a X'PERT-PRO X-Ray diffractometer equipped with a Ni filter and operated at 40 kV and 40 mA. The samples were scanned from an initial value of 2θ = 5° to a final value of 2θ = 80°, with a step size of 0.026° and a counting time of 26.8 s. From the obtained diffractograms, the cell parameter of the $Co_3O_4$ phase was obtained by full profile matching using FullProf.2k software. On the other hand, the Raman spectra of the samples were obtained with Renishaw InVia Raman spectrometer, coupled to a Leica DMLM microscope, with an ion-argon laser (Modu-Laser, 514 nm). For each sample, five scans in the spectral window of 150–900 $cm^{-1}$ and a spatial resolution of 2 μm were accumulated. Finally, XPS measurements were performed in a Kratos AXIS Supra spectrometer using a 225 W Al Kα radiation source with a pass energy of 20 eV.

The redox properties of the catalysts were investigated on a Micromeritics Autochem 2920 apparatus coupled to a TCD detector by means of Temperature-Programmed Reduction with hydrogen ($H_2$-TPR) and Temperature-Programmed Reaction with methane ($CH_4$-TPRe). In both cases an initial pre-treatment step with a 5%$O_2$/He mixture at 300 °C for 30 min was performed with the aim of removing impurities form the surface of the samples while at the same time fully restoring the oxygen vacancies of the spinel lattice before the analysis of the reducibility. After cooling down to room temperature with flowing He, the experiments were conducted up to 600 °C, with a 5%$H_2$/Ar mixture and a 5% $CH_4$/He mixture, respectively. In the $CH_4$-TPRe the composition of the gaseous stream was monitored with a MKS Cirrus Quadrupole Mass Spectrometer.

### 2.3. Experimental reaction set-up

The efficiency of the foam catalysts for the complete oxidation of dilute methane was examined in a fixed bed quartz tubular (10 mm ID) reactor in the 200–600 °C temperature range with a heating rate of 1 ºC $min^{-1}$. The runs were carried out with a single piece of foam catalysts (with a mass of 650–700 mg) that were deposited on a glass frit located near the bottom of the reactor tube. The GHSV calculated on the basis of the total volume of the foam catalyst (1.5 ml) was around 4000 $h^{-1}$. This corresponded to a WHSV of 85 l $g_{Co3O4}{}^{-1}$ $h^{-1}$. In order to avoid gas channelling each structured catalyst was wrapped with an aluminium foil. Light-off tests were repeated at least three times to assure reproducibility, with an average 12 h of use for each structured catalyst. The composition of the feed stream was 1%$CH_4$/10%$O_2$/89%$N_2$ with a total flow of 100 ml $min^{-1}$. Note that the typically encountered $O_2/CH_4$ molar ratio can vary between 2 and 6 for stoichiometric engines and between 10 and 70 for lean engines. The used ratio in this work falls within this last range. The composition of the reaction gases was continuously analysed by a SRS RGA200 quadrupole mass spectrometer following the $m/z$ = 44 ($CO_2$), 32 ($O_2$), 28 (CO) and 16 ($CH_4$) signals. The analysis of the product stream was carried out in steps of 25 ºC, typically after 15 min on stream. Each analysis was performed in triplicate in order to check reproducibility. A margin of error of less than 1% was found. Methane conversion was determined by the difference between inlet and outlet $CH_4$ molar flows. Additionally, the effect of the presence of water (10–30%vol.) and carbon dioxide (10%vol.) on the catalyst stability with time on stream was investigated at constant temperature (550 ºC) for a total reaction interval of 285 h. The influence of GHSV in the 4000–60,000 $h^{-1}$ range (85–850 l $g_{Co3O4}{}^{-1}$ $h^{-1}$) was also studied.

## 3. Results and discussion

### 3.1. Assessment of SCS as a suitable route for preparing efficient $Co_3O_4$ catalysts

The suitability of SCS as an attractive methodology for producing efficient cobalt catalysts for lean methane oxidation was initially addressed. Thus, a bulk $Co_3O_4$ oxide was obtained using cobalt nitrate as precursor and glycine as fuel (Φ = 1). As aforementioned, the reactive mixture was heated at 250 °C for 30 min in order to activate the SCS reaction. The resulting sample was then calcined at 600 °C for 4 h. For comparative purposes, a reference $Co_3O_4$ catalyst was synthesised by simple calcination of the same cobalt precursor under identical thermal conditions (600 °C/4 h). Both samples were prepared without cerium as promoter. Their performance in the oxidation of methane was examined at 30 l $g_{Co3O4}{}^{-1}$ $h^{-1}$ in the 200–600 °C temperature range. The composition of the feedstream was 1%$CH_4$/10%$O_2$/89 $N_2$%. Three consecutive light-off runs were recorded. While a slight decrease in activity with temperature was observed in the second run with respect to the first run, the third light-off curve was virtually identical to the second run. Hence, the light-off curves corresponding to the third cycle of each catalyst are shown in Fig. 1. It was found that the sample synthesised with glycine showed a $T_{50}$ (temperature at which 50% conversion was attained) of 455 °C, while its counterpart required 480 °C. 90% conversion was obtained at 525 and 575 °C, respectively. A significantly higher reaction rate under differential conditions (375 °C) was also noticed (1.2 vs 0.8 mmol $CH_4$ $g_{Co3O4}{}^{-1}$ $h^{-1}$). It must be pointed out that despite the fact that the reaction rate, on a surface area basis, of the sample prepared by calcination is twice that of the one prepared by SCS, the calcination method cannot produce catalysts with high specific surface areas, and therefore with a large population of active sites.

The superior oxidation ability of the sample prepared by SCS was connected with its appreciably better textural properties although no significant difference in the crystallite size were found (84–89 nm). Hence, the increased volume of gases produced during the fuel-assisted combustion process provoked a higher porosity as revealed by the larger surface area (14 vs 5 $m^2$ $g^{-1}$) and pore volume (0.04 vs 0.02 $cm^3$ $g^{-1}$) and the smaller mean pore size (170 vs 355 Å). Likewise, a favoured reducibility at low temperatures was observed over the oxide synthesised with glycine as revealed by $H_2$-TPR (Fig. S2, Supplementary Material). It was found that the onset reduction temperature was 280 °C compared with 300 °C. Besides, the $H_2$ uptake at low temperatures

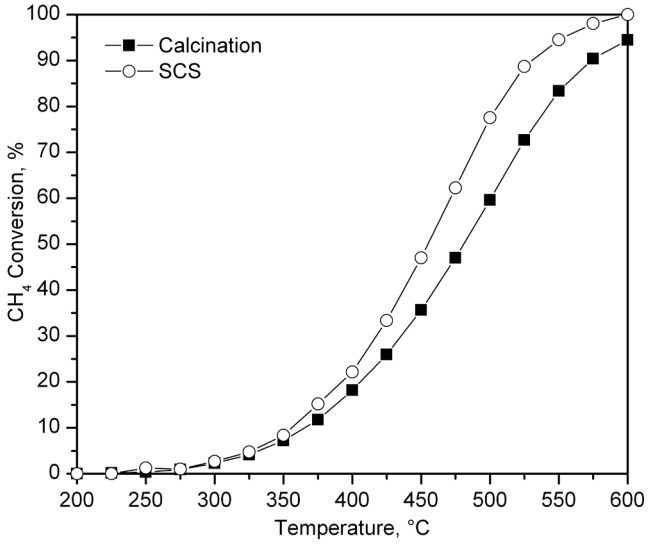


**Fig. 1.** Light-off curves of the bulk $Co_3O_4$ catalysts prepared by solid combustion synthesis (SCS) with glycine (Φ = 1) and direct calcination (DC).

(250–325 °C) was markedly larger 3.9 vs 2.6 mmo $g^{-1}$). In sum, this preliminary catalytic evaluation accompanied by the characterisation of the textural and redox properties evidenced the potential of the combustion route aided by a fuel (glycine) for preparing promising oxidation cobalt catalysts [30,31], and therefore justifies a deeper analysis for its optimisation in the removal of lean methane. As stated earlier, our interest will be now focused on the investigation of this methodology for intensifying the methane oxidation process with highly active Ce-promoted cobalt catalysts supported on open-cell α-$Al_2O_3$ foams. In this sense, it must highlighted that the use of low amounts of Ce as an additive has been observed to promote the performance of cobalt catalysts notably since it increases the mobility of active oxygen species [27, 28].

### 3.2. Synthesis of the Ce-Co foam catalysts

For defining the number of cycles required to achieve the desired amount of $CeO_2$-modified $Co_3O_4$ (approximately 10%wt.$Co_3O_4$ and 1% wt.$CeO_2$, which corresponded to a Ce/Co molar ratio of 0.05) loaded onto the foam substrate, the evolution of the $Co_3O_4$ oxide mass concentration as function of the number of cycles is shown in Fig. S3, Supplementary Material. This graph includes the mean oxide concentration for each cycle, which was estimated from gravimetric measurements by the difference of the coated and base foams prepared in duplicate with both fuels and the entire Φ range (0.25–1.0). Thus, 16 measurements were averaged for each cycle. Hence, the consecutive cycles led to a gradual increase in $Co_3O_4$ concentration from about 1% (1st cycle), 2% (2nd cycle), 6% (3rd cycle) to 10% (4th cycle). It is worth pointing out that irrespective of the synthesis conditions (type of fuel and Φ ratio) the amount of oxides coated in each cycle was quite reproducible. Hence, four cycles were tentatively required to attain the target concentration (10%wt.$Co_3O_4$). It must be pointed out that the metal concentration by chemical analysis was not determined after each coating step, since that would have destroyed the sample after the corresponding coating step. Therefore, the actual metallic loadings were determined by ICP-AES was only measured for the foam catalysts coated after four consecutive runs. As will be shown later on, a significantly lower metallic content was found with respect to that expected from gravimetric measurements although the Ce/Co molar ratio was always equal to nominal value (0.05).

On the other hand, the adhesion of the catalytic coating onto the open cell foams was examined by ultrasonic treatment. Several samples were submerged in a 50% isopropanol/50% water solution and subjected to sonication at 40 kHz and 200 W for 1 h in a Selecta ULTRASONS-H ultrasonic cleaner. Before and after the test, the samples were dried at 110 °C for 1 h and weighted to measure the mass loss owing to the sonication treatment. These tests revealed a minimal mass loss (0.2–0.4%wt.) after the sonication treatment, thus suggesting that the utilised combustion route was adequate to obtain structured samples with a relatively high mechanical stability of the deposited Ce-Co oxide.

### 3.3. Characterisation of the Ce-Co foam catalysts

SEM analysis of the foam catalysts was carried out to ascertain differences in the morphology and homogeneity of the Ce-Co coating as function of the used fuel. Thus, Fig. 2 and Fig. S4, Supplementary Material include representative SEM images of the two samples prepared with urea and glycine with Φ = 1, along with images of the pristine foam. Note that the surface morphology of the bare foam substrate was rough and consisted of an agglomeration of crystallites with various sizes and shapes, probably due to the foam being a mixture of several ceramic materials. Complementary EDX analysis was performed for semi-quantitatively estimating the elemental composition of the catalyst surface (a depth of 0.5–1 μm). Thus, around 65 spot analyses on selected regions of both samples were carried out. Attention was paid to estimating the Co/Al molar ratio as a criterion for comparing the dispersion of cobalt on the foam, and more importantly, the Ce/Co molar ratio for characterising the contact between these two metals. Fig S5 (Supplementary material) shows the relative distribution of this ratio at the surface of the foam catalysts.

After depositing the Ce-Co catalyst with urea, the formation of a distinct catalytic layer could not be distinguished. In fact, the observed structural morphology (x1300 magnification) was rather similar to that of the bare foam. The averaged Co/Al molar ratio derived from EDX was

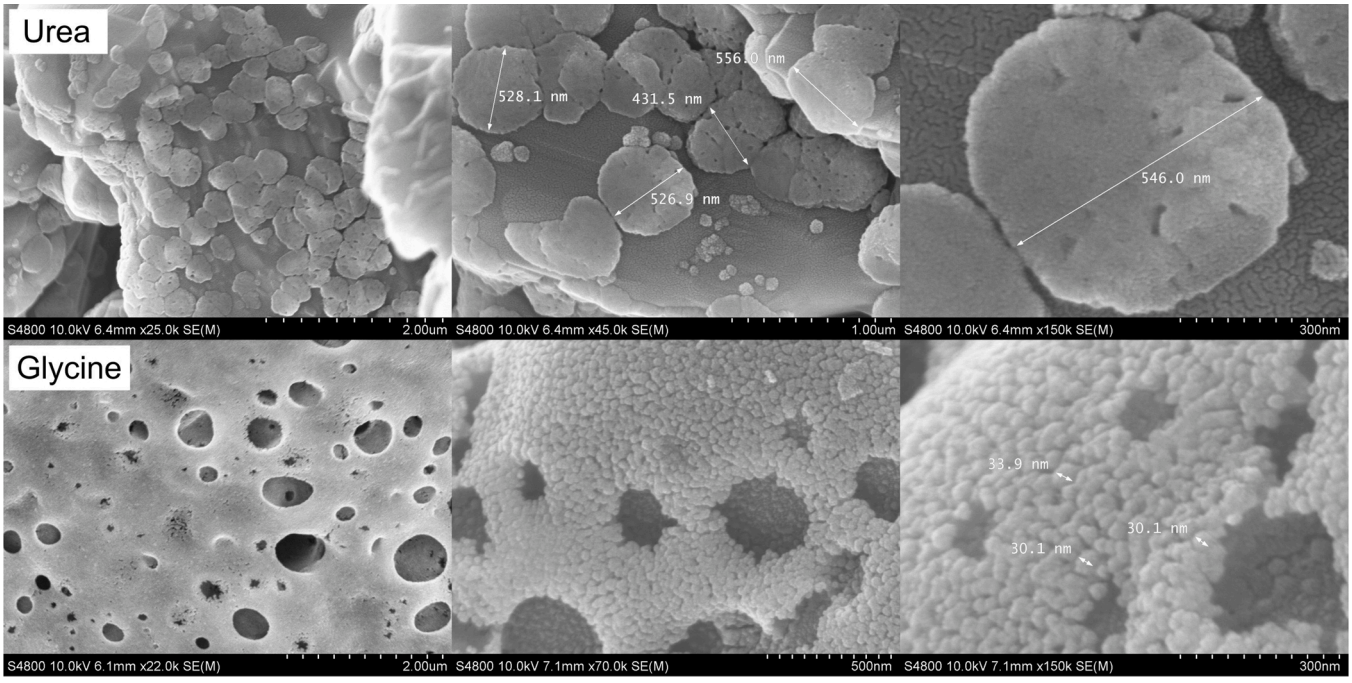


**Fig. 2.** High magnification (x22,000–150,000) SEM images of the foam catalysts prepared with Φ = 1. (a-c) F(U) catalyst (a) x25,000 (b) x45,000 (c) x150,000; (d-f) F(G) catalyst (d) x22,000 (e) x70,000 (f) x150,000.

very low, around 0.06, which evidenced a relatively poor accessibility of cobalt species located on the surface of the foam. Although the mean Ce/Co molar ratio (0.06) was close to that determined by ICP-AES (0.05), a great variability in the relative abundance was detected on various regions of the catalyst, which suggested a non-homogenous distribution of these two metals. Hence, Ce-rich areas were identified on some regions (25% and 12% of the spot analysis evidenced a Ce/Co molar ratio higher than 0.06 and 0.1, respectively), while other zones were characterised by a low concentration of cerium species (43% of the spot analysis revealed a Ce/Co molar ratio lower than 0.03). On the other hand, high-magnification SEM images (x25,000–150,000) shown in Fig. 1 revealed that the surface was covered by round patches with sizes ranging 450–500 nm, although some smaller clusters of around 50–200 nm were also visible. Likewise, uncovered areas of foam could be observed.

Conversely, when the catalyst was prepared with glycine the surface of the foam substrate was not visible due to being fully covered with a clearly observable catalytic layer, which in addition presented a porous, foamy morphology with large voids in its microstructure. Judging from the images at medium magnification (x1300–1800), the oxides were homogeneously deposited and well anchored on the structured support although superficial debris were also found (Fig. 2). On average, the estimated Co/Al molar ratio derived from spot EDX measurements was around 1.3, substantially higher than that of the urea-based counterpart (0.06). This suggested a better distribution of cobalt on the surface of the foam. On the other hand, a transversal cut from a piece of this catalyst (Fig. S5, Supplementary Material) revealed that the thickness of the catalytic coating was around 7 μm, with a part of the deposited cobalt being able to filter through the pores among the ceramic particles of the foam substrate. By zooming in on the foamy microstructure of the layer (x22,000–150,000) it was observed that it was actually formed by the aggregation of crystallites around 25–30 nm in size. The spongy structure and the relatively small $Co_3O_4$ crystallite were assigned to the easier and more violent combustion of the glycine nitrate gel and to the large amount of gases released during the combustion process that simultaneously inhibited sintering and favoured the creation of a porous network [32–34]. As for the relative abundance of cerium and cobalt species, the measured mean Ce/Co molar ratio was 0.06, close to the nominal value (0.05), thereby revealing an intimate mixing of both elements. Interestingly, almost 95% of the spot analysis evidenced a Ce/Co molar ratio between 0.05 and 0.06, which suggested a homogeneous relative distribution of both metals on the surface of the foam.

Complementary HAADF-STEM coupled to EDX mapping was useful to determine the differences in the spatial distribution of cobalt and cerium on the surface of these two foam catalysts (Fig. 3). This analysis required a previous crushing of the foams until obtaining a fine powder. As already noted, the surface of the urea-prepared sample was sparsely covered with bulky patches of catalytic material. Furthermore, both cobalt and cerium species were generally present as isolated entities, with very low mixing between the two metals. Therefore, it was clearly evidenced that the dispersion of both cobalt and cerium was certainly poor. In contrast, in the case of catalyst F(G), the surface of the foam was completely covered with both metals. Moreover, the cerium species exhibited good dispersion and mixing with cobalt, with almost no segregated clusters of ceria. These results evidenced the appreciably better structural properties of the supported catalyst prepared with glycine with respect to the urea-based counterpart.

The crushed samples were also investigated by ICP-AES, $N_2$ physisorption, XRD, HRTEM, Raman spectroscopy, XPS, $H_2$-TPR and $CH_4$-TPRe, with the aim of studying the effect of the type of fuel and Φ ratio on the physico-chemical properties of the deposited metal oxides. Firstly, the composition of the samples after the fourth SCS cycle was determined by ICP-AES. The corresponding results are given in Table 1. A slightly lower oxide loading was detected (6.8–8.8%wt.$Co_3O_4$ and 0.80–1.01%wt.$CeO_2$) when compared with the estimate given by

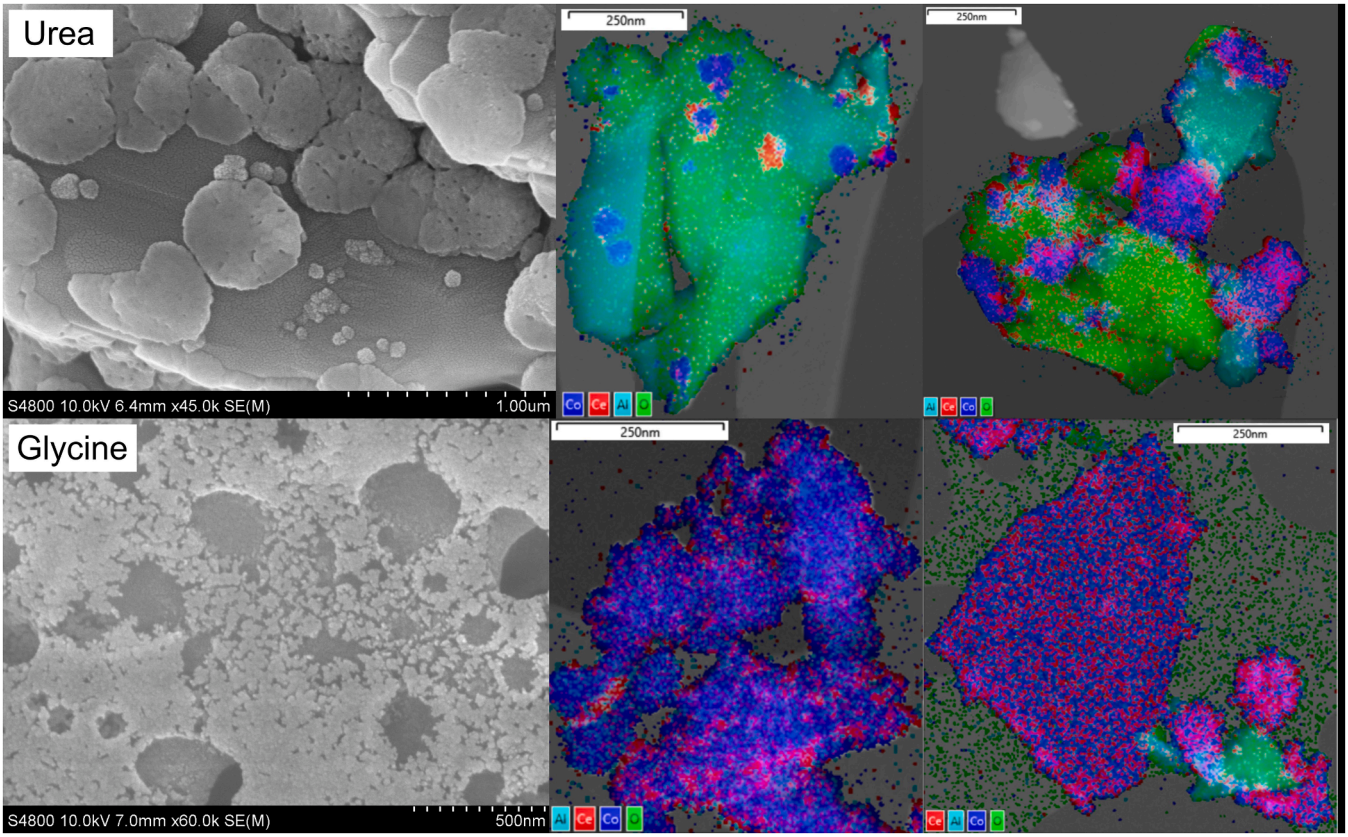


**Fig. 3.** SEM and HAADF-STEM images of the foam catalysts prepared with Φ = 1, coupled with EDX elemental distribution of Co (dark blue), Ce (red), Al (light blue) and O (green). (For interpretation of the references to colour in this figure, the reader is referred to the web version of this article.)

**Table 1**
Composition and $Co_3O_4$ and $CeO_2$ crystallite size of the foam catalysts after four SCS cycles.

| | F (U) catalysts | | | | F (G) catalysts | | | |
|---|---|---|---|---|---|---|---|---|
| Catalyst | $Co_3O_4$, %w | t.$CeO_2$, %wt. | $D_{Co3O4}$, nm | $D_{CeO2}$, nm | $Co_3O_4$, %w | t.$CeO_2$, %wt. | $D_{Co3O4}$, nm | $D_{CeO2}$, nm |
| $\Phi = 0.25$ | 7.9 | 0.88 | 50 | 12 | 8.2 | 0.92 | 28 | 7 |
| $\Phi = 0.50$ | 8.7 | 0.99 | 52 | 12 | 7.8 | 0.86 | 24 | 8 |
| $\Phi = 0.75$ | 8.8 | 1.01 | 50 | 10 | 7.2 | 0.82 | 18 | 8 |
| $\Phi = 1.00$ | 7.8 | 0.87 | 47 | 10 | 6.8 | 0.80 | 18 | 7 |

thermogravimetric measurements. Nevertheless, the actual Ce/Co molar ratio of all foam catalysts determined by chemical analysis was virtually identical to that expected theoretically (0.05). On the other hand, by means of Raman spectroscopy, the possible presence of carbonaceous species derived from the thermal decomposition of organic fuels during the SCS process was examined. Hence, the absence of the signals at about 1340 and 1580 $cm^{-1}$ assigned to the so-called D and G bands [35] suggested that the combustion reaction of the fuel was complete. Accordingly, the observed mass loss of the samples by dynamic thermogravimetry (10 °C $min^{-1}$, Setaram Setsys Evolution) up to 900 °C under oxidative conditions was negligible.

The textural properties of the ceramic substrate and the two foam catalysts prepared with glycine and urea ($\Phi = 1$) were compared. BET measurements of the bare foam were expected to reveal its macroporous character with a very low surface area (about 0.2 $m^2\ g^{-1}$). Interestingly, an appreciable increase in surface area up to 2 $m^2\ g^{-1}$ was found for the F(G) catalyst. This finding was consistent with the porosity of the deposited oxide catalyst as observed by SEM analysis. An estimate of the intrinsic surface area of the metallic phase resulted in around 26 $m^2\ g^{-1}$. By contrast, the surface area (0.6 $m^2\ g^{-1}$) of the F(U) catalyst was close to that of the blank substrate. The X-Ray diffractograms (with a step size of 0.026° and a counting time of 2.0 s) of all structured catalysts are shown in Fig. 4. The diffraction pattern of the bare foam substrate was also included for the sake of comparison. Its pattern was characterised by the intense signals of the trigonal phase of the alpha-alumina support ($2\theta$ = 25.7, 37.8, 43.5, 52.6, 57.6, 61.4, 66.6, 68.4 and 77.0°) (ICDD 01–081–1667). However, it must be pointed out that additional signals were noticed, which were assigned to impurities such as mullite (ICDD 01–074–2419) at $2\theta$ = 16.5, 23.7, 26.3, 31.0, 33.3, 35.3, 37.1, 39.3, 41.0, 42.7, 49.5, 54.2, 60.8, 64.7, 70.5 74.4 and 75.2°; cristobalite (ICDD 01–076–0935) at $2\theta$ = 21.9, 46.4, 48.5 and 36.1° and cordierite (ICDD 01–084–1221) at $2\theta$ = 10.5, 28.4 and 29.6°, as can be seen in Fig. S6, Supplementary Material. The set of signals corresponding to the presence of the cobalt spinel oxide ($Co_3O_4$) at $2\theta$ = 19.0, 31.3, 36.8, 38.5, 44.8, 59.4 and 65.2° (ICDD 00–042–1467) were identified for all foam catalysts. The presence of CoO or Co that could be formed by reduction of $Co_3O_4$ in the presence of the organic fuel was ruled out. Also, a weak signal at $2\theta$ = 28.6°, attributable to the cubic phase of segregated $CeO_2$ (ICDD 00–004–0593), was visible. Accordingly, HRTEM images of the samples prepared with $\Phi = 1$ (Fig. S7, Supplementary Material) allowed the resolution of lattice fringes of $Co_3O_4$ (0.29 and 0.24 nm, which corresponded to the {220} and the {311} planes, respectively) and $CeO_2$ crystallites (0.31 and 0.27 nm, which corresponded to the {111} and {200} planes, respectively). The observation of the latter oxide phase suggested that a fraction of cerium was not incorporated into the framework of the cobalt spinel. The mean crystallite size of $Co_3O_4$, determined by the Scherrer equation, was around 50 nm for the catalysts prepared with urea and between 19 and 28 nm for the F(G) catalysts (Table 1). Apparently, these sizes were not greatly influenced by the used $\Phi$ ratio for each fuel, and were in the same range as those reported by Toniolo et al. [36] for $Co_3O_4$ oxides synthesised with glycine (23–37 nm) and urea (50–77 nm) with varying $\Phi$ (0.25–1). On the other hand, a comparison of this crystallite size with that estimated by SEM analysis evidenced that the $Co_3O_4$ particles observed in the sample prepared with urea, unlike those present in the glycine-based counterpart, were formed by the apparent agglomeration of smaller crystallites.

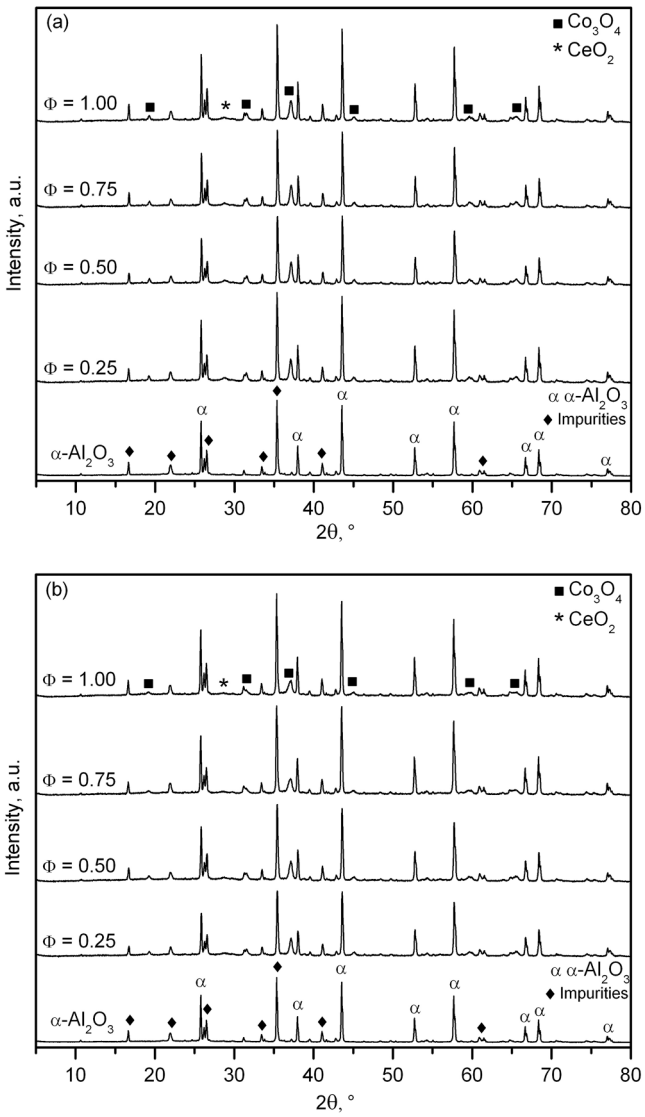


**Fig. 4.** X-Ray patterns of the foam catalysts prepared with urea (a) and glycine (b).

Finally, as indicated above, the introduction of cerium into the lattice of the cobalt spinel was not complete since relatively small crystallites of cerium oxide were observed. The estimated size of $CeO_2$ crystallites ranged between 10 and 12 and 7–8 nm for the F(U) and F(G) catalysts, respectively. The extent of insertion of cerium atoms into the lattice of $Co_3O_4$ could be qualitatively evaluated by analysing its cell parameter, as shown in Fig. 5. The cell parameter was calculated via a full profile fitting of the high-resolution diffractograms by using FullProf.2k software. In principle, a larger value could be associated with a greater abundance of cerium atoms given the larger ionic radii of $Ce^{4+}$ (101 pm)

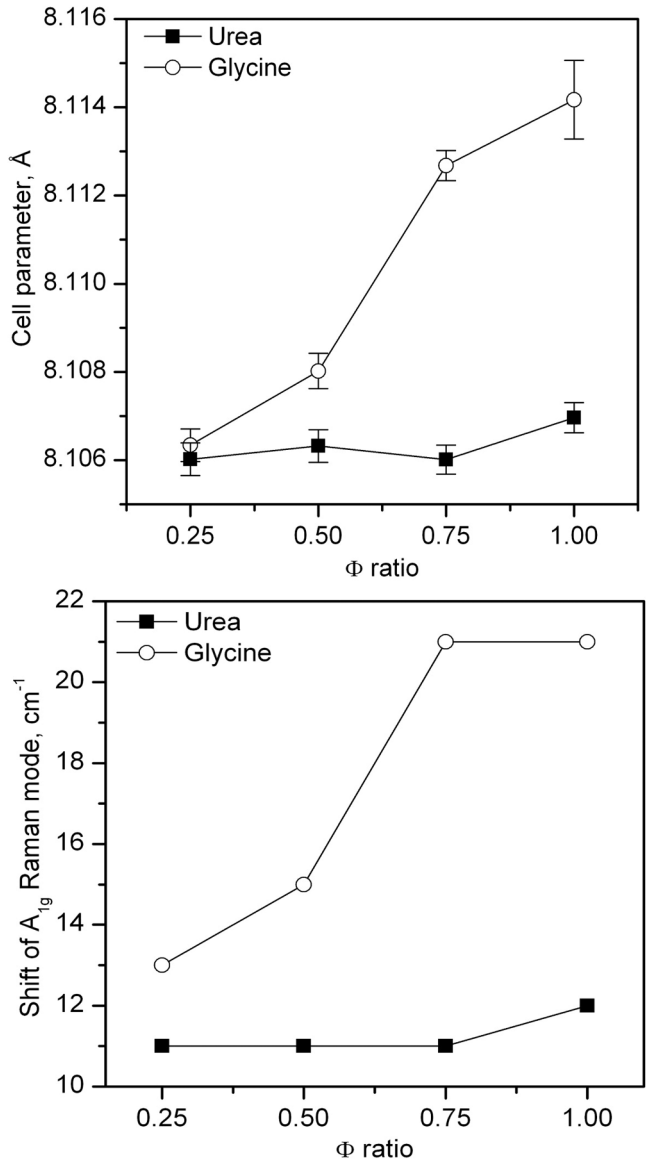


**Fig. 5.** Evolution of the $Co_3O_4$ cell parameter and the shift of the $A_{1\,g}$ Raman vibration mode of the foam catalysts with the Φ ratio.

and $Ce^{3+}$ (115 pm) compared with $Co^{3+}$ (69 pm) and $Co^{2+}$ (79 pm). As a reference, the cell parameter of the bulk $Co_3O_4$ sample prepared by SCS (glycine) was estimated (8.0988 Å). Regarding the F(U) samples, it was significantly larger (8.1060–8.1070 Å) although no appreciable differences were noticed with varying Φ ratio. However, in the case of the F (G) samples the insertion of cerium atoms was substantially promoted, and highly dependent on the used amount of glycine. Thus, the cell parameter was 8.1210 Å for the sample with $\Phi = 1$. The distortion of the spinel structure caused by cerium as a function of the synthesis conditions (type and amount of fuel) was also followed by Raman spectroscopy. In this way, a shift of the main Raman bands could be taken as an evidence of the extent of this structural change. The Raman spectra of the F(U) and F(G) catalysts are shown in Fig. S8, Supplementary Material. The spectra of the bulk Ce-free $Co_3O_4$ sample was also included for comparative purposes as it was taken as a reference to examine the eventual shift corresponding to the Ce-modified foam catalysts. This pure oxide exhibited the five expected vibrations of the $Co_3O_4$ lattice, namely three bands at 187, 506 and 602 $cm^{-1}$ from the $F_{2\,g}$ vibration modes, an $E_g$ vibration mode at 462 $cm^{-1}$ and finally a signal at 667 $cm^{-1}$ attributed to the $A_{1\,g}$ vibration mode [37]. Fig. 4 includes the observed shift of the latter band ($A_{1\,g}$) as a function of the Φ ratio for both fuels. As for the F(U) samples, the shift was similar for all samples (11–12 $cm^{-1}$), thereby revealing that cerium insertion was not favoured with increasing amounts of urea. However, when using glycine the shift was more marked (13–21 $cm^{-1}$). The results evidenced a greater distortion of the lattice, particularly for $\Phi = 1$. To sum up, both XRD and Raman results suggested that the SCS route was suitable for partially doping the lattice of cobalt oxide, and that the extent of cerium insertion and the subsequent lattice distortion was favoured when large amounts ($\Phi = 0.75$–1) of glycine were used. Although the possible insertion of cobalt into the ceria lattice could not be ruled out, this could not be evidenced by XRD and Raman spectroscopy, probably due to the low cerium content of the samples.

The surface chemical state of the foam catalysts was investigated by XPS. Hence, the near-surface composition and distribution of cobalt, cerium, and oxygen species was determined by deconvolution and integration of the $Co2p_{3/2}$ (777–792 eV), Ce3d (881–917 eV) and O1s (526–536 eV) spectra, respectively, as shown in Fig. S9, Supplementary Material. Additionally, the Al2p and Si2p spectra were integrated to include these elements in the surface elemental composition. The surface charging effect in the spectra was compensated against the C-H states in the C 1 s spectra with the energy assumed to be 284.6 eV. As shown in Table 2, it was found that cerium tended to be located preferentially on the surface of the samples with a concentration that was approximately ten times higher (7.8–9.1%wt.) than the corresponding bulk concentration (0.7–0.8%wt.) estimated by ICP-AES. This accumulation could be ascribed to low surface energy of cobalt species compared to ceria, which in turn results in the favoured presence of ceria on the outer surface. Therefore, Ce/Co molar ratios in the 0.22–0.38 range were observed in the foam catalysts.

The $Co2p_{3/2}$ spectra were deconvoluted into three main contributions and two satellites. The first two main components, centred at 779.5 and 780.6 eV, were attributed to the existence of $Co^{3+}$ and $Co^{2+}$ ions, respectively, while the third one, centred at 782.3 eV, was assigned to the presence of $Co^{2+}$ as CoO [38]. Typically, the contribution of the latter component was less than 10% of the total surface Co concentration. This oxide was presumably formed due to in situ partial reduction of surface $Co_3O_4$ species under vacuum conditions in the XPS spectrometer. Therefore, it could be assumed that this phase was not present in the catalyst formulation. The signals located at 785.2 and 789.4 eV were identified as the shake-up satellite peaks of the $Co^{2+}$ and $Co^{3+}$ ions, respectively [39]. It must be pointed out that the position of the main

**Table 2**
Surface composition of the foam catalysts.

| F (U) catalysts | Co, %wt. | Ce, % wt. | Ce/ Co | $Co^{3+}$/ $Co^{2+}$ | $Ce^{3+}$/ $Ce^{4+}$ | $O_{latt}$/ $O_{tot}$ |
|---|---|---|---|---|---|---|
| $\Phi = 0.25$ | 10.2 (5.8) | 8 (0.7) | 0.33 | 0.80 | 0.40 | 0.11 |
| $\Phi = 0.50$ | 10.1 (6.4) | 9.1 (0.8) | 0.38 | 0.93 | 0.33 | 0.11 |
| $\Phi = 0.75$ | 12.1 (6.4) | 9 (0.7) | 0.31 | 0.90 | 0.32 | 0.10 |
| $\Phi = 1.00$ | 9.6 (5.7) | 7.8 (0.7) | 0.34 | 0.84 | 0.35 | 0.11 |
| **F(G) catalysts** | | | | | | |
| | Co, %wt. | Ce, % wt. | Ce/ Co | $Co^{3+}$/ $Co^{2+}$ | $Ce^{3+}$/ $Ce^{4+}$ | $O_{latt}$/ $O_{tot}$ |
| $\Phi = 0.25$ | 10.3 (6.0) | 9 (0.8) | 0.37 | 0.93 | 0.33 | 0.11 |
| $\Phi = 0.50$ | 15.1 (5.7) | 9.9 (0.7) | 0.28 | 1.05 | 0.25 | 0.13 |
| $\Phi = 0.75$ | 17 (5.3) | 9.5 (0.7) | 0.24 | 1.06 | 0.26 | 0.15 |
| $\Phi = 1.00$ | 18.3 (5.0) | 9.7 (0.7) | 0.22 | 1.08 | 0.23 | 0.21 |

Values in parentheses correspond to the bulk composition as determined by ICP-AES.

bands as well as their satellite bands did not vary markedly among all foam catalysts. Nevertheless, the deconvolution of the Co2p$_{3/2}$ band in the components from $Co^{2+}$ and $Co^{3+}$ suggested notable differences in the oxidation state of cobalt on the surface. Hence, as a general behaviour it was observed that the $Co^{3+}/Co^{2+}$ molar ratio of the F(U) samples was slightly lower (0.80–0.93) compared with the F(G) counterparts (0.83–1.08). It was then possible to establish that smaller crystallites sizes were characterised by the presence of more oxidised cobalt species. On the other hand, it was also remarkable that for the samples prepared with the lowest amount of fuel ($\Phi = 0.25$) were characterised by the lowest $Co^{3+}/Co^{2+}$ molar ratio. This was reasonably connected with the severe substoichiometric conditions of the combustion synthesis. In contrast, higher amounts of fuel resulted in a favoured presence of $Co^{3+}$ species.

On the other hand, the O1s spectra were deconvoluted into four signals (Fig. S9, Supplementary Material). The first two contributions, located at 529.7 and 531.0 eV, were assigned to the lattice oxygen species from the cobalt oxide and the ceramic substrate, respectively. The third signal, centred at 532.1 eV, was attributed to weakly adsorbed oxygen species on the surface of the samples. Note that these oxygen species could be located indistinctively on the surface of both the ceramic support and the Ce-Co active phase. Finally, the last signal, located at 533.0 eV was attributed to the presence of carbonates, water and hydroxyl species [40]. Given the high ability of lattice oxygen species of Co-based catalysts for methane oxidation [41], its relative abundance was estimated as the $O_{latt}/O_{tot}$ molar ratio for all samples. The amount of $O_{latt}$ species was assumed to be proportional to the area under the signal peaking at 529.7 eV. It is noteworthy that the estimated amount of adsorbed oxygen species may be affected by air exposure. However, it is highly likely that this contamination did not result in a remarkable effect on the quantification of the amount of lattice oxygen species, since those are strongly bonded to Co or Ce atoms. Consequently, the $O_{latt}/O_{total}$ molar ratio of all samples would be overestimated. However, since all catalyst exhibited comparable specific surface areas, that overestimation could be assumed to be similar between all samples. Therefore the comparison among the various samples would be meaningful. Regarding the F(U) catalysts, this ratio barely varied with the $\Phi$ ratio with values around 0.10–0.11. However, a significantly higher ratio was found for the F(G) samples, which notably depended on the $\Phi$ ratio. Thus, it increased from 0.11 ($\Phi = 0.25$) to 0.21 ($\Phi = 1$). In sum, the use of increasing amounts of glycine as fuel favoured the presence of oxygen lattice species in the resulting Ce-Co oxide, which in turn was strongly related to the abundance of $Co^{3+}$ ions (Fig. S10, Supplementary Material).

To define the eventual relationship between the distribution of cerium species and the $Co^{3+}/Co^{2+}$ molar ratio, the Ce3d spectra of all samples were fitted with eight peaks corresponding to four pairs of spin-orbit doublets (Fig. S9, Supplementary Material). Following the convention adopted by Murugan et al. [42], letters U and V were used to refer to the 3d$_{5/2}$ and 3d$_{3/2}$ spin-orbit components, respectively. Of the four pairs of peaks, three of them (namely V, U; V'', U'' and V''', U''') were associated with electrons from $Ce^{4+}$ while the remaining pair (V′, U′) was attributed to electrons from $Ce^{3+}$ species. The $Ce^{3+}/Ce^{4+}$ molar ratios were obtained from the areas of the 3d$_{5/2}$ and 3d$_{3/2}$ components for each species. It must be noted that the estimation of this ratio could be affected by the possibility of cerium reduction under the conditions of spectra recording, thereby resulting in an overestimation of the proportion of $Ce^{3+}$. Although it was difficult to quantify the extent of this eventual reduction, and since the samples were submitted to the same experimental analysis conditions and the ceria particle size of the foam catalysts was relatively similar (7–12 nm), it was assumed that the samples of the same set of foam catalysts (F(G) or F(U)) would exhibit a similar tendency to form $Ce^{3+}$. Therefore the estimated $Ce^{3+}/Ce^{4+}$ molar ratios could at least qualitatively compared. It was found that this ratio decreased as the $Co^{3+}/Co^{2+}$ molar ratio increased, which could be explained in terms of the equilibrium $Ce^{3+}+Co^{3+} \leftrightarrow Ce^{4+}+Co^{2+}$ established by the charge balance requirement within the cations of the spinel lattice [43]. Hence, an increase in $Co^{3+}$ population at the expense of $Co^{2+}$ resulted in a decrease of $Ce^{3+}$ ions in favour of $Ce^{4+}$.

$H_2$-TPR analysis was used to characterise the reducibility of the foam catalysts, since this is one of the main parameters governing the performance of $Co_3O_4$-based catalysts in redox reactions. A 5%$H_2$/Ar mixture was used as the reducing gas and the experiments were carried out with a heating ramp of 10 ºC min$^{-1}$ between 50 and 900 ºC. Fig. 6 shows the corresponding reduction patterns (up to 600 ºC) of the samples prepared with the two fuels and varying $\Phi$ ratio. It should be pointed out that the observed $H_2$ consumption would correspond to the reduction of deposited cobalt and cerium species, which is expected to occur simultaneously. In order to decouple the reduction process of $Co^{3+}$, $Co^{2+}$ and $Ce^{4+}$ cations, our attention will be first paid to analysing the reducibility of cobalt species. Regardless the synthesis conditions, the reduction process of all catalysts was dominated by a main reduction event at around 350 ºC and a more or less perceptible signal at lower temperatures (300 ºC). Thus, the onset temperature was approximately 250 °C and 300 °C for F(G) and F(U) samples, respectively. These findings were in accordance with the sequential reduction of $Co^{3+} \rightarrow Co^{2+} \rightarrow Co^0$ [44]. It must be pointed out that above 400 °C no significant

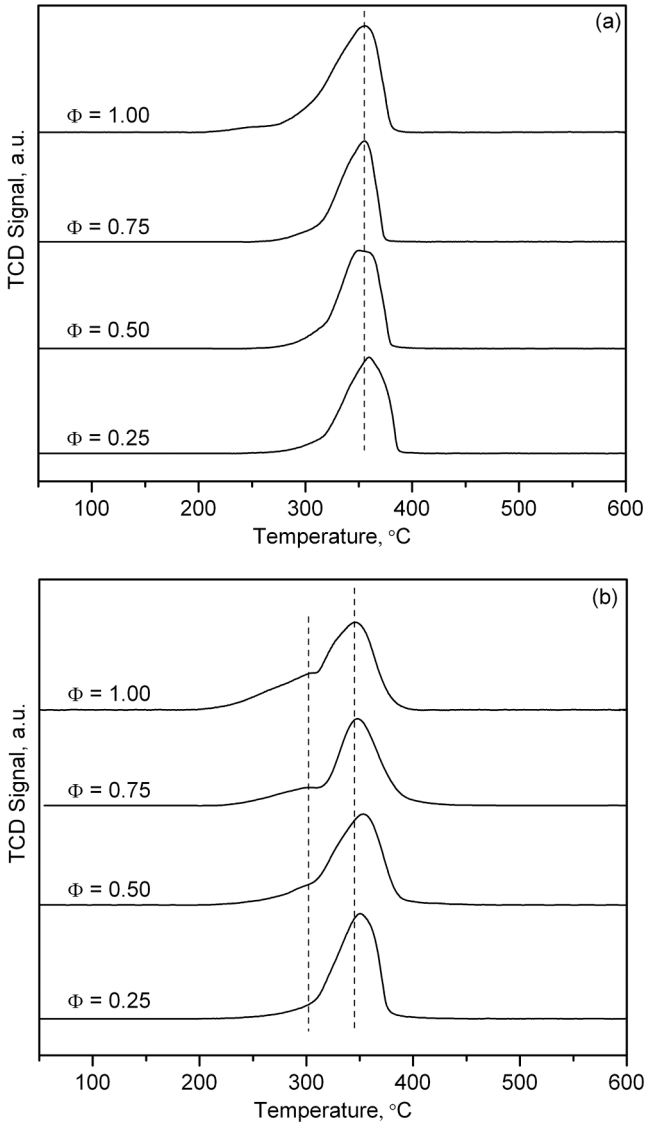


**Fig. 6.** $H_2$-TPR profiles of the foam catalysts prepared with urea (a) and glycine (b).

**Table 3**
Specific $H_2$ uptake of the foam catalysts.

| Catalyst | F (U) catalysts | | F (G) catalysts | |
|---|---|---|---|---|
| | Low-temperature $H_2$ uptake, mmol $gCo_3O_4^{-1}$ | High-temperature $H_2$ uptake, mmol $gCo_3O_4^{-1}$ | Low-temperature $H_2$ uptake, mmol $gCo_3O_4^{-1}$ | High-temperature $H_2$ uptake, mmol $gCo_3O_4^{-1}$ |
| $\Phi = 0.25$ | 1.47 | 15.26 | 2.09 | 14.83 |
| $\Phi = 0.50$ | 1.57 | 15.17 | 2.94 | 14.08 |
| $\Phi = 0.75$ | 1.52 | 15.25 | 3.64 | 13.42 |
| $\Phi = 1.00$ | 1.75 | 15.19 | 4.12 | 13.01 |

$H_2$ uptake was observed, which ruled out the presence of highly stable cobalt species in the form of cobalt aluminate [45]. This was coherent with the high chemical stability of alpha alumina that prevented the formation of this undesired spinel.

After integrating the profiles of the F(G) samples (Table 3) it was found that the total specific $H_2$ uptakes were in all cases higher than those theoretically expected (16.6 mmol $g_{Co3O4}^{-1}$), thereby suggesting the appreciable contribution to the overall reducibility of the cerium species present in the samples, mainly inserted in the spinel lattice as $Ce^{4+}$ cations. The reduction of these species was expected to occur in the same temperature window (250–400 °C) as cobalt species and could be activated due to the transfer of hydrogen by metallic cobalt onto the ceria [46]. The $H_2$ uptake ranged between 16.9 and 17.1 mmol $g_{Co3O4}^{-1}$, and apparently depended on the amount of fuel used in the synthesis. These results would be in agreement with a favoured incorporation of cerium with high Φ ratios, as suggested by XRD and Raman spectroscopy. The contribution of $Ce^{4+}$ reduction to the overall reducibility of the Ce-Co catalysts was evaluated by analysing a post-run sample, particularly the one prepared with $\Phi = 1$, by XPS. Thus, it was observed that its $Ce^{3+}/Ce^{4+}$ molar ratio substantially increased from 0.23 over the fresh sample to 0.44. On the other hand, the improvement in the redox properties of the samples prepared with increasing amounts of glycine was also reflected in the shift of the reduction temperatures to lower values. Furthermore, when taking a temperature of 300 °C as a criterion, the low-temperature uptake increased with the Φ ratio, from 2.1 mmol $g_{Co3O4}^{-1}$ for $\Phi = 0.25$–4.1 mmol $g_{Co3O4}^{-1}$ for $\Phi = 1$. As for the F(U) catalysts, their total $H_2$ uptake was comparable (16.7–16.9 mmol $g_{Co3O4}^{-1}$), and slightly larger than the theoretical consumption. This suggested that the amount of cerium species in the lattice was comparable irrespective of the Φ ratio, in line with the results given by XRD and Raman spectroscopy. The low-temperature uptake was rather similar (1.5–1.7 mmol $g_{Co3O4}^{-1}$) for all F(U) catalysts, and appreciably lower in comparison with their glycine-based counterparts. Analogously, a post-run sample (the one prepared with $\Phi = 1$) was characterised by XPS. In this case, no marked differences in its $Ce^{3+}/Ce^{4+}$ molar ratio were found (0.35 for the fresh sample and 0.40 for the sample after the $H_2$-TPR run). Finally, it must be pointed out only the diffraction signals of metallic cobalt were clearly distinguished (ICDD 00–015–0806) for both used catalysts. No signals related to cerium species were visible. This was expected due to the low Ce content as $CeO_2$ (lower than 1%wt. $CeO_2$) of the samples.

In addition to $H_2$-TPR, the intrinsic reactivity of the oxygen species present in each set of foam catalysts was also characterised by studying the ability of a given sample for oxidising methane (5%$CH_4$/He) in the absence of oxygen with increasing temperature ($CH_4$-TPRe). These experiments were conducted up to 600 ºC with a heating rate of 10 ºC $min^{-1}$ followed by an isothermal step for 30 min. The amounts of evolved $CO_2$ ($m/z = 44$) as the main oxidation product and CO ($m/z = 28$) and $H_2$ ($m/z = 2$) as by-products derived from possible reforming processes during the run were measured. These results can be helpful in understanding the lean methane oxidation reaction in the light of the widely accepted Mars – van Krevelen mechanism. As shown in Fig. S11 (Supplementary Material), the process is dominated by the large formation of $CO_2$ (and CO and $H_2$, not shown) at 600 °C that corresponded to the full reduction of cobalt species, which eventually catalysed the conversion of methane into syngas and $CO_2$. However, more valuable data could be extracted from the detected production of $CO_2$ at lower temperatures (400–550 °C), since this could be exclusively ascribed to the full oxidation of methane by the active oxygen species of the Co-Ce foam catalysts. Thus, an enlarged view of the $CO_2$ generation profile in this temperature window is included in Fig. 7. It was observed that for the F(U) catalysts the reactivity of oxygen species was relatively similar in view of their comparable peak oxidation temperature around 525–530 °C, except for the sample prepared with a Φ ratio of 0.25 (550 °C). In addition, a comparable oxygen consumption was observed from this set of samples ranging between 0.31 and 0.35 mmol $O_2$ $g_{Co}^{-1}$. The onset temperature for methane oxidation was in the 415–455 °C range. The onset temperature was defined as the temperature at which 5% of the total $CH_4$ uptake in the low temperature range (below 550 ºC) was consumed. Interestingly, the catalysts prepared with glycine were considerably more active as revealed by the lower onset (380–415 °C) and peak oxidation temperatures (495–535 °C). Also, more appreciable was the amount of oxygen species involved in the oxidation process over

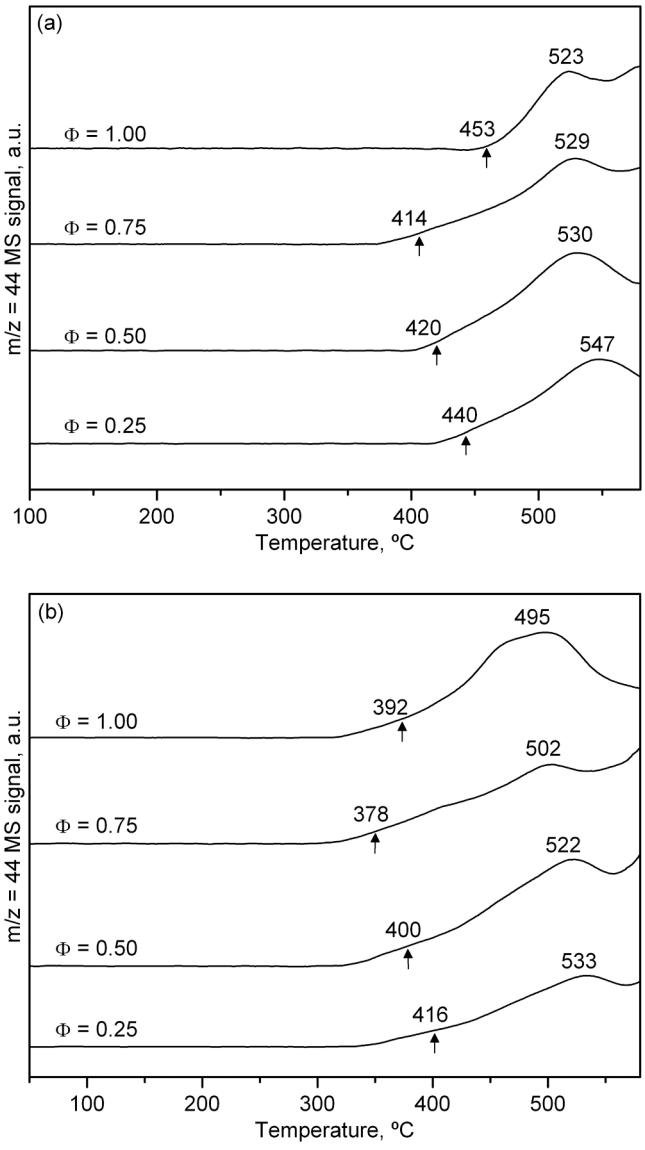


**Fig. 7.** $CH_4$-TPRe profiles in the 100–580 °C temperature range of the foam catalysts prepared with (a) urea and (b) glycine.

these samples that ranged between 0.31 and 0.56 mmol $O_2$ $g_{Co}^{-1}$. All the results suggested that the use of glycine produced samples with improved properties for methane oxidation that could be associated with the favoured oxygen mobility induced by cerium insertion in the $Co_3O_4$ lattice. Thus, the most promising samples were the foam catalysts prepared with high Φ ratios (0.75 and 1.00).

### 3.4. Catalytic activity of the open cell foams structured catalysts

Fig. 8 shows the corresponding light-off curves of the oxidation of lean methane (85 l $g_{Co3O4}^{-1}$ $h^{-1}$) over the foam catalysts prepared with each fuel and varying Φ ratio. The GHSV was around 4000 $h^{-1}$, calculated based on the total volume of structured foam catalyst (1.5 ml). Carbon dioxide and water were the only detected reaction products. The absence of mass and heat transfer limitations within the reactor was checked in order to ensure that they did not affect the obtained kinetic results. Taking into account that the transfer regimes for a structured catalyst significantly varies with respect to their powdered counterparts, four different criteria were checked following the recommendations given by Ercolino et al. [16] and Italiano et al. [47], namely Carberry (external mass transfer), Weisz-Prater (internal mass transfer), Mears (external heat transfer) and Anderson (internal heat transfer) criteria.

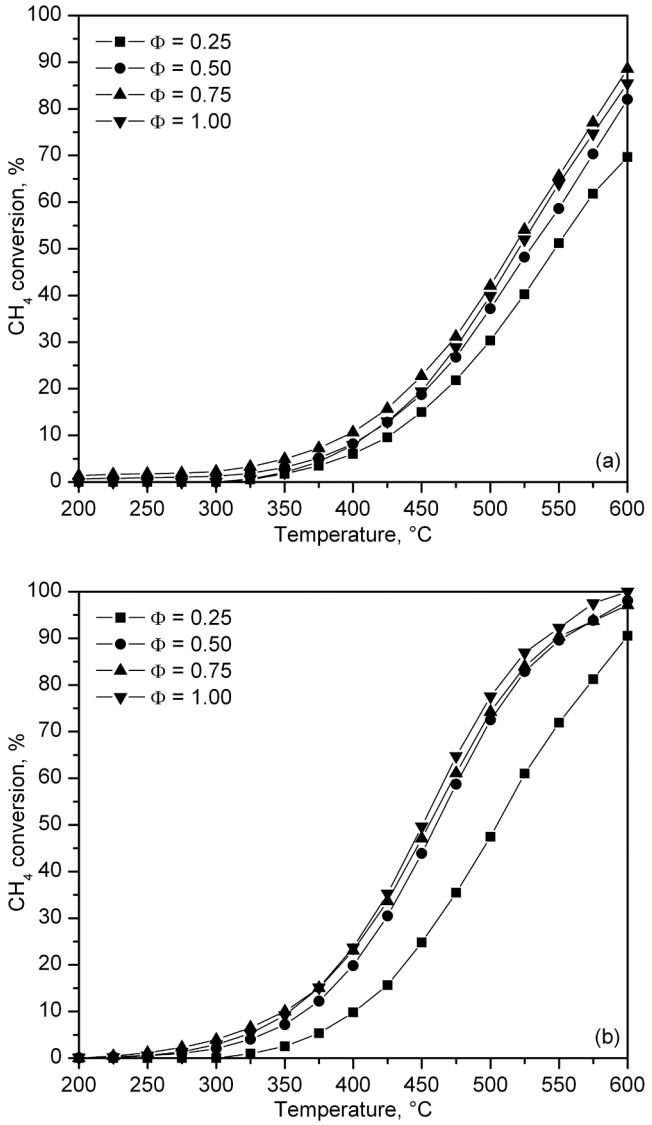


**Fig. 8.** Light-off curves of the foam catalysts with urea (a) and glycine (b).

The mathematical equations related to each criterion are listed in Table S2, Supplementary Material. As an example, corresponding values derived from the estimated reaction data at several temperatures (300–600 °C) for the foam catalyst prepared with glycine and Φ = 1 are included in this table. Judging from the obtained results it was verified that inter- and intra-phase concentration and temperature gradients were negligible below 500–550 ºC. Note that the contribution of heat/mass transfer limitations expectedly was significant at high temperatures (600 ºC) since the estimated values were only one order of magnitude lower with respect to the corresponding threshold.

As for the foam catalysts synthesised with urea, an appreciable conversion (10%) was noticed at 400–425 °C. In view of the $T_{50}$ values (Table 4) the foam samples with a Φ = 0.75 and Φ = 1.0 showed a similar efficiency with values in the 515–520 °C range, whereas the sample with Φ = 0.5 required 530 °C for this conversion level (50%). Clearly, the poorest performance was shown by the catalyst prepared with the lowest amount of urea (Φ = 0.25). Accordingly, the conversion trend at 600 °C followed the same order, namely, 85% conversion (Φ = 0.75–1.0), 80% conversion (Φ = 0.5) and 70% conversion (Φ = 0.25). By contrast, the use of glycine as a fuel comparatively resulted in markedly more efficient foam catalysts. Hence, at 400–425 °C a conversion as high as 20% was already noticed. No substantial differences were observed among the samples with a Φ ratio of 1.0 ($T_{50}$ = 450 °C), 0.75 ($T_{50}$ = 455 °C) and 0.5 ($T_{50}$ = 460 °C), as shown in Table 4. Thus, these three samples achieved at least 95% conversion at 600 °C. Again, the catalyst prepared with the lowest Φ ratio exhibited a considerably poorer performance ($T_{50}$ = 500 °C).

Despite the differences in activity found among the foam catalysts obtained with both fuels, the apparent activation energies of all examined samples were in the 70–76 kJ $mol^{-1}$ range. These values were comparable to those exhibited by bulk $Co_3O_4$ oxides [48,49], and suggested that the obtained kinetic results were not affected by diffusional limitations, in line with the results reported in Table S2, Supplementary Material. The apparent activation energy was estimated by assuming a first pseudo-order for methane and a zeroth pseudo-order for oxygen [50]. The integral method was applied to estimate the apparent activation energy when considering a first pseudo-order for methane and a zero pseudo-order for oxygen. Conversions between 10% and 90% were fit to the following linearized equation for the integral reactor (Eq. 1)

$$\ln[-\ln(1-X)] = \ln\left[k_0 C_{CH_{40}}\left(\frac{W}{F_{CH_{40}}}\right)\right] - \frac{E_a}{RT} \quad (1)$$

where X is the fractional conversion of methane, $k_0$ is the pre-exponential factor of the Arrhenius equation and $W/F_{CH40}$ is the weight hourly space velocity. The goodness of the numerical fit is shown in Fig. S12 (Supplementary material).

Having proven that glycine was a more suitable fuel for depositing the active phases on the open cell foams by solid combustion synthesis, the determination of the optimal Φ ratio was attempted by comparing the specific reaction rate at a selected temperature of 400 °C. This reaction rate was calculated under differential conditions (conversion<20%). Therefore, it was estimated as the ratio between the experimental conversion and the weight hourly space velocity (W/

**Table 4**
Kinetic results of the foam catalysts.

| Catalyst | F (U) catalysts | | | F (G) catalysts | | |
|---|---|---|---|---|---|---|
| | $T_{50}$, °C | ($-r_A$) @ 400 °C, mmol $CH_4$ $g_{Co3O4}^{-1}$ $h^{-1}$ | Ea, kJ $mol^{-1}$ | $T_{50}$, °C | ($-r_A$) @ 400 °C, mmol $CH_4$ $g_{Co3O4}^{-1}$ $h^{-1}$ | Ea, kJ $mol^{-1}$ |
| Φ = 0.25 | 545 | 1.3 | 72 ± 2 | 505 | 1.9 | 76 ± 2 |
| Φ = 0.50 | 530 | 1.3 | 73 ± 1 | 460 | 3.8 | 74 ± 1 |
| Φ = 0.75 | 515 | 1.9 | 71 ± 2 | 450 | 4.8 | 70 ± 2 |
| Φ = 1.00 | 520 | 1.7 | 74 ± 1 | 450 | 5.3 | 71 ± 2 |

$F_{CH40}$). Results included in Table 4 and Fig. 8 revealed a notable dependence of the intrinsic activity with the amount of fuel for the F(G) catalysts. Hence, the normalised reaction rate notably increased from 1.9 (Φ = 0.25) to 3.8 mmol $CH_4$ $g_{Co3O4}$ $h^{-1}$ (Φ = 0.5). This promotion, although less noticeable, was also evident with larger amounts of fuel. In this way, the foam catalyst prepared with the highest Φ ratio (Φ = 1) exhibited a reaction rate of 5.3 mmol $CH_4$ $g_{Co3O4}$ $h^{-1}$. For comparative purposes, obtained results of the catalysts prepared with urea were included in Fig. 9 as well. As dictated by the light-off curves, the intrinsic activity at 400 °C was remarkably lower, in the 1.3–1.9 mmol $CH_4$ $g_{Co3O4}$ $h^{-1}$ range. The differences in performance among the various examined Φ ratios were rather less obvious when using this fuel.

A reasonable correlation was found between the low-temperature $O_2$ consumption of the foam catalysts, as determined by $CH_4$-TPRe analysis, and their specific reaction rate (Fig. 10). This relationship would be the confirmation of the methane oxidation reaction followed a Mars – van Krevelen mechanism, since the catalysts that exhibited larger $O_2$ uptakes due to their favoured mobility of oxygen species evidenced a higher catalytic activity. The reason for this behaviour seemed to lie on the larger abundance of $Co^{3+}$ ions on the surface of the catalysts prepared with high Φ ratios of glycine, which in turn resulted in a more abundant presence of lattice oxygen species with high mobility, as evidenced by the complementary correlations depicted in Fig. 9 among the normalised reaction rate and the $Co^{3+}/Co^{2+}$ and $O_{latt}/O_{tot}$ at the surface. The superior performance of the glycine-based catalysts prepared with glycine with respect to their urea-based counterparts was ultimately associated with a more efficient insertion of cerium into the lattice of the spinel, thus promoting the presence of $Co^{3+}$ ions within it. This induced a more marked distortion that led to improved redox properties at low temperatures. Structurally the F(G) catalysts also exhibited a well anchored, homogeneous catalytic coating on the surface of the ceramic substrate characterised by a good dispersion of both cobalt and cerium, and a relatively high porosity.

The performance of the most active catalyst, namely the sample synthesised with glycine and a Φ = 1, was studied at varying GHSV in the 4000–60,000 $h^{-1}$ range (equivalent to a WHSV in the 85–1275 l $g_{Co3O4}^{-1}$ $h^{-1}$ range) at 600 ºC. Results included in Fig. S13 (Supplementary material) correspond to the averaged conversion for 4 h in steps of 4000 $h^{-1}$. Expectedly, a gradual decrease in conversion was found at lower residence times, from 95% at 4000 $h^{-1}$, to 82% at 16,000 $h^{-1}$ and 72% at 60,000 $h^{-1}$. Interestingly, upon returning to the baseline GHSV (4000 $h^{-1}$) and after a total accumulated time interval of 56 h at 600 °C, the conversion recovered to the same initial value (close to 95%), thereby suggesting a reasonably good thermal stability of the foam catalyst.

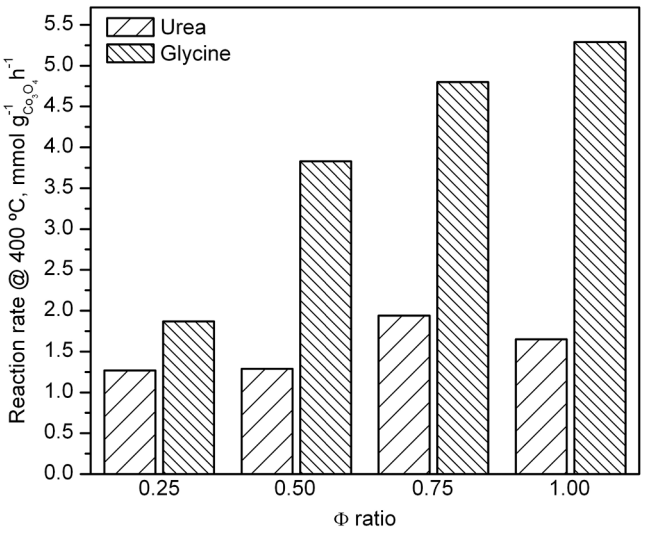


**Fig. 9.** Relationship between the specific reaction rate of the foam catalysts and the Φ ratio.

Additionally, the effect of the presence of water (10%vol.) and carbon dioxide (10%vol.) on the catalyst stability with time on stream was investigated under isothermal conditions (550 ºC) for a total reaction interval of 285 h (85 l $g_{Co3O4}^{-1}$ $h^{-1}$). Firstly, the following feed mixtures were alternated every 25 h: 1%$CH_4$/10%$O_2$/$N_2$ - 1%$CH_4$/10%$O_2$/10%$CO_2$/$N_2$ - 1%$CH_4$/10%$O_2$/$N_2$ - 1%$CH_4$/10%$O_2$/10%$H_2O$/$N_2$ - 1%$CH_4$/10%$O_2$/$N_2$ - 1%$CH_4$/10%$O_2$/10%$H_2O$/10%$CO_2$/$N_2$. Finally, conversion was again recorded under a 1%$CH_4$/10%$O_2$/$N_2$ atmosphere (5 h). The evolution of methane conversion under these reaction conditions is included in Fig. 11. During the first 25 h of operation, the samples showed a marked thermal stability with no evidence of deactivation. Hence, a relatively constant conversion at around 86% was noticed. After the subsequent admission of carbon dioxide to the feedstream during additional 25 h, conversion was hardly affected. Upon returning to base conditions, the same conversion was still maintained. However, the addition of water caused a significant decrease to a stable value of 58% due its adsorption on the catalyst surface. Interestingly, when water was subsequently cut off, the methane conversion was almost fully recovered, with a value similar (82%) to that observed under dry conditions. Thus, it was evidenced that this temporary inhibiting effect of water did not lead to a significant irreversible deactivation of the sample. Finally, attention was paid to examining the effect of the simultaneous presence of carbon dioxide and water for 25 h in an attempt to mimic a real exhaust gas from a natural gas-fuelled engine. Interestingly, the decrease in conversion provoked by water was not accentuated to a greater extent when combined with carbon dioxide, since a mean conversion of 56% was noted. When returning to the base conditions (1% $CH_4$/10%$O_2$/$N_2$) the mean conversion along 5 h was 81%.

After the first 155 h with alternating conditions, the influence of the presence of larger amounts of water vapour in the feed stream was then analysed. For this reason, varying concentrations of water vapour, from 10% to 30%vol. were admitted into the reactor during consecutive periods of 25 h. It was found that, despite the high used concentrations, the detrimental effect to the methane conversion was relatively limited. Hence, the average conversions for the various water vapour concentrations were 53% (15%$H_2O$), 50% (20% $H_2O$), 47% (25% $H_2O$) and 45% (30% $H_2O$), thus evidencing that the catalyst was relatively resistant to increased concentrations of water in the feed stream. Moreover, after returning to the base dry conditions, the achieved conversion was 78%, which pointed out that the irreversible deactivation phenomenon was also limited even after exposure of the catalyst to a feedstream containing 30%$H_2O$. It must be pointed out that the eventual formation of CO and $H_2$ derived from reforming processes of methane (steam and/or dry reforming) was not observed. Even in the presence of 10%$CO_2$ and up to 30%$H_2O$ the selectivity to $CO_2$ was 100%. In other words, it could be assumed that the reactivity of methane with oxygen (10%) was highly preferential, even when admixtured with water vapour (30%) and/or $CO_2$(10%).

The (fresh) catalyst was subjected to a similar stability test as well, but operating at under a higher space velocity, in order to assess the influence of water vapour in conditions closer to those found in real natural gas engines exhausts. During consecutive reaction time intervals of 25 h at 600 ºC, the catalytic performance was evaluated under dry and humid conditions (10–30%H2O) at 4000 $h^{-1}$ (85 l $g_{Co3O4}^{-1}$ $h^{-1}$) and 40,000 $h^{-1}$ (850 l $g_{Co3O4}^{-1}$ $h^{-1}$). Results shown in Fig. S14 (Supplementary material) for the first 100 h were in agreement with the previous results on stability (Fig. 10). Hence, the conversion under dry conditions at 4000 $h^{-1}$ was around 95%, decreasing to 77% when adding 10%$H_2O$ and recovering again to the initial value after cutting off the admission of water. When the water concentration was raised to 30%vol. the conversion decreased to 59%. As for the second 100 h-time interval at higher space velocity, the negative effect of the addition of water was found to be less marked with respect to that observed at 4000 $h^{-1}$, probably due to the water having a shorter residence time to

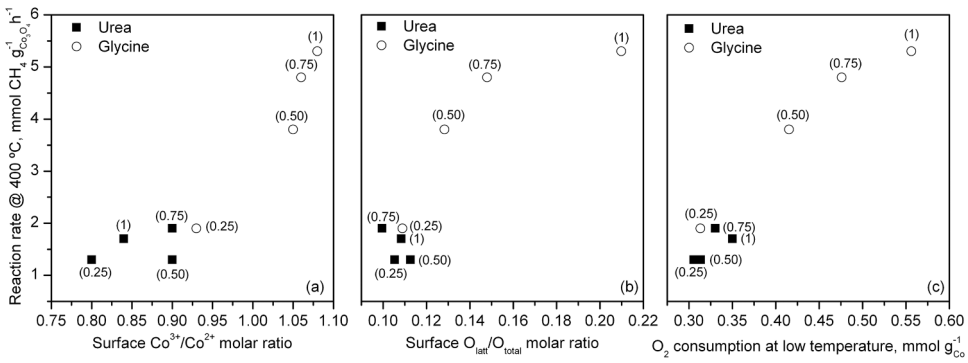


**Fig. 10.** Relationship between the (a) surface $Co^{3+}/Co^{2+}$ molar ratio, (b) surface $O_{latt}/O_{tot}$ molar ratio and (c) low-temperature $O_2$ consumption from the $CH_4$-TPRe runs, and the specific reaction rate of the foam catalysts. Values in parenthesis correspond to the Φ ratio.

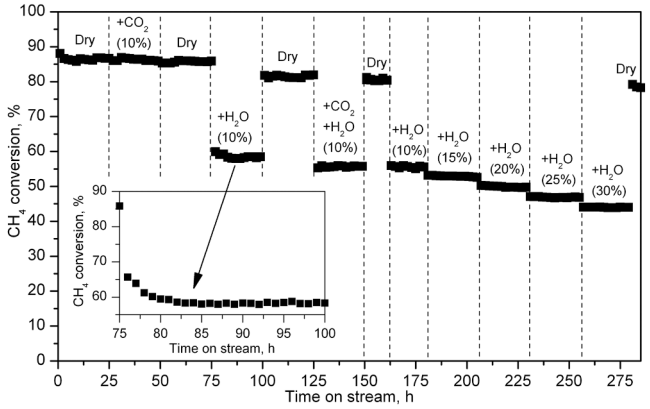


**Fig. 11.** Evolution of methane conversion with time on stream over the F(G) catalyst prepared with $\Phi = 1$ at 85 l $g_{Co3O4}^{-1}$ $h^{-1}$ and 550 °C under varying reaction conditions. The $CH_4$ and $O_2$ concentration was fixed at 1% and 10%, respectively.

adsorb on the surface of the catalyst. Thus, under the dry conditions the average conversion was 73% and decreased to 58% with 10%$H_2O$ and to 48% in the presence of 30%$H_2O$.

Finally, the catalyst subjected to the 285 h-stability test (at 550 °C and 4000 $h^{-1}$ in the presence of $H_2O$ and $CO_2$) was characterized in order detect any structural or chemical differences with its fresh counterpart, which could be responsible for the slight deactivation caused by the long term exposure to water vapour. Thus, XRD analysis found no abnormal crystalline phases in the aged catalyst, although the estimated average $Co_3O_4$ crystallite size was found to be appreciably larger (32 nm vs. 18 nm). On the other hand, when comparing SEM images (Fig. S15, Supplementary material), a notable deterioration of the superficial structure was detected in the used sample, with multiple cracks and rifts that spread from the numerous pores of the original foamy structure. Images taken at high magnification also confirmed the results given by XRD, with the $Co_3O_4$ crystallites exhibiting poorly defined borders and generally larger sizes (35–55 nm). These findings evidenced that exposure to water vapour induced a slight sintering.

The spent catalyst was also submitted to $CH_4$-TPRe analysis in order to assess the effect of water vapour ageing on the redox properties and mobility of oxygen species. The profile of $CO_2$ production ($m/z = 44$) of both fresh and used catalysts, shown in Fig. S16 (Supplementary material), revealed a marked worsening in the reducibility of the used sample, given the increase in both the onset reduction temperature, from 392° to 412 °C, and in the peak reduction temperature, from 495° to 500 °C. However, after integration of the profiles it was found that the low-temperature $O_2$ consumption of both samples was identical (0.56 mmol $O_2$ $g_{Co}^{-1}$). Thus, the decrease in the reducibility of the used sample was merely a side effect of the aforementioned sintering of the $Co_3O_4$ crystallites, and not due to any detrimental effect on the intrinsic chemical properties of the catalyst. This was in line with the identical Ce/Co molar ratio (0.06) found by EDX on the surface of both fresh and used samples.

## 4. Conclusions

In this work the intensified lean methane oxidation with novel $Co_3O_4$(10 wt%)-$CeO_2$(1 wt%) catalysts supported over α-$Al_2O_3$ open cell foams was investigated. The structured catalysts were prepared by solution combustion synthesis using urea or glycine as fuel while varying the fuel/oxidiser ratio (Φ ratio) between 0.25 and 1.0. The textural, structural, morphological and redox properties were examined by a wide number of analytical techniques including SEM-EDX, STEM-HAADF coupled to EDX mapping, ICP-AES, WDXRF, $N_2$ physisorption, XRD, HRTEM, Raman spectroscopy, XPS, $H_2$-TPR and $CH_4$-TPRe. The catalytic performance was evaluated under realistic reaction conditions in terms of a relatively high gas hourly space velocity and the simultaneous presence of water and carbon dioxide in the exhaust gas of the natural gas fuelled vehicle.

Glycine was found to produce catalysts with a considerably better performance than the urea-based counterparts, with specific reaction rates being around 3 times higher. From a structural and morphological point of view, the reason behind this behaviour was closely related to the intrinsic porosity of the Ce-Co catalytic layer deposited onto the foam substrate, relative dispersion of deposited cobalt and cerium species and the $Co_3O_4$ crystallite size resulting from the used type of fuel. In particular, the catalysts prepared with glycine resulted in the formation of a highly porous catalytic coating containing relatively small, well dispersed spherical oxide crystallites. In contrast, the samples synthesised with urea did not lead to the formation of a distinct, homogeneous Ce-Co layer. In fact, some areas of the foam were not fully covered while other areas presented large flat patches of cobalt oxide. Moreover, the intimate mixture of cobalt and cerium when using glycine as fuel allowed for a more efficient insertion of Ce ions into the lattice of the cobalt spinel, which translated into a more favoured presence of $Co^{3+}$ ions within the $Co_3O_4$ structure. This, in turn, led to an increased presence and mobility of the lattice oxygen species that led to a better performance for lean methane oxidation. The optimal fuel/oxidiser ratio for glycine was found to be the stoichiometric one. This foam catalyst exhibited a notable activity even at low residence times. Moreover, this sample showed a marked thermal and hydrothermal stability under isothermal conditions (550–600 ºC). While the catalytic performance was not affected by the presence of carbon dioxide, the observed inhibiting effect of water was found to be almost reversible, although exposure to humid conditions eventually caused an appreciable sintering of the $Co_3O_4$ crystallites.

## CRediT authorship contribution statement

**Andoni Choya:** Investigation, Writing – original draft. **Sylwia Gudyka**: Investigation. **Beatriz de Rivas:** Methodology, Validation. **Jose Ignacio Gutiérrez-Ortiz:** Methodology, Formal analysis. **Andrzej Kotarba**: Methodology, Conceptualization. **Ruben López-Fonseca:** Conceptualization, Writing – review & editing, Supervision.

## Declaration of Competing Interest

The authors declare that they have no known competing financial interests or personal relationships that could have appeared to influence the work reported in this paper.

## Acknowledgements

This work was supported by the Spanish Ministry of Science and Innovation [PID2019–107105RB-I00 AEI/FEDER, UE]; the Basque Government [IT1297–19]; and the University of the Basque Country UPV/EHU [PIF15/335 and DOCREC21/23]. The technical and human support provided by Advanced Research Facilities-SGIker (UPV/EHU), and Central Scientific and Technological Research Services/Atomic Spectroscopy Division (University of Cádiz) is acknowledged. In addition, authors acknowledge the use of instrumentation as well as the technical advice provided by the National Facility ELECMI ICTS, node 'Advanced Microscopy Laboratory' at University of Zaragoza.

## Appendix A. Supporting information

Supplementary data associated with this article can be found in the online version at doi:10.1016/j.apcata.2022.118511.

## References

[1] A. Thiruvengadam, M. Besch, V. Padmanaban, S. Pradhan, B. Demirgok, Energy Policy 122 (2018) 253–259, https://doi.org/10.1016/j.enpol.2018.07.052.
[2] D. Jiang, K. Khivantsev, Y. Wang, ACS Catal. 10 (2020) 14304–14314, https://doi.org/10.1021/acscatal.0c03338.
[3] P. Li, R. Zhang, X. Wang, S. Liu, N. Liu, B. Chen, Mol. Cat. 437 (2017) 26–36, https://doi.org/10.1016/j.mcat.2017.04.024.
[4] F. Zasada, J. Grybos, E. Budiyanto, J. Janas, Z. Sojka, J. Catal. 371 (2019) 224–235, https://doi.org/10.1016/j.jcat.2019.02.010.
[5] B. Feng, M. Shi, J. Liu, X. Han, Z. Lan, H. Gu, X. Wang, H. Sun, Q. Zhang, H. Li, Y. Wang, H. Li, J. Hazard. Mater. 394 (2020), 122540, https://doi.org/10.1016/j.jhazmat.2020.122540.
[6] T.M. Nyathi, N. Fischer, A.P.E. York, M. Claeys, ACS Catal. 10 (2020) 11892–11911, https://doi.org/10.1021/acscatal.0c02653.
[7] E.M. Iwanek, L.F. Liotta, G. Pantaleo, K. Krawczyk, E. Gdyra, J. Petryk, J. W. Sobczak, Z. Kaszkur, Catalysts 11 (2021) 1–13, https://doi.org/10.3390/catal11030325.
[8] G. Grzybek, S. Wójcik, K. Ciura, J. Gryboś, P. Indyka, M. Oszajca, P. Stelmachowski, S. Witkowski, M. Inger, M. Wilk, A. Kotarba, Z. Sojka, Appl. Catal. B Environ. 210 (2017) 34–44, https://doi.org/10.1016/j.apcatb.2017.03.053.
[9] Z. Liu, L. Cheng, J. Zeng, X. Hu, S. Zhangxue, S. Yuan, Q. Bo, B. Zhang, Y. Jiang, Chem. Phys. 540 (2021), 110984, https://doi.org/10.1016/j.chemphys.2020.110984.
[10] L. Xing, Y. Yang, W. Ren, D. Zhao, Y. Tian, T. Ding, J. Zhang, L. Zheng, X. Li, Catal. Today 351 (2020) 83–93, https://doi.org/10.1016/j.cattod.2018.12.009.
[11] S. Hosseini, H. Moghaddas, S.M. Soltani, S. Kheawhom, Process Saf. Environ. 133 (2020) 286–300, https://doi.org/10.1016/j.psep.2019.11.020.
[12] D. Wang, Q. Chen, X. Zhang, C. Gao, B. Wang, X. Huang, Y. Peng, J. Li, C. Lu, J. Crittenden, Environ. Sci. Technol. 55 (2021) 2743–2766, https://doi.org/10.1021/acs.est.0c07326.
[13] Y. Chen, N. Wang, O. Ola, Y. Xia, Y. Zhu, Mater. Sci. Eng. R Rep. 143 (2021), 100589, https://doi.org/10.1016/j.mser.2020.100589.
[14] M.V. Twigg, J.T. Richardson, Ind. Eng. Chem. Res. 46 (2007) 4166–4177, https://doi.org/10.1021/ie061122o.
[15] D. Ciria, M.P. Orihuela, J.A. Becerra, R. Chacartegui, J. Ramírez-Rico, Fuel 304 (2021), 121264, https://doi.org/10.1016/j.fuel.2021.121264.
[16] G. Ercolino, P. Stelmachowski, S. Specchia, Ind. Eng. Chem. Res. 56 (2017) 6625–6636, https://doi.org/10.1021/acs.iecr.7b01087.
[17] A. Klegova, A. Inayat, P. Indyka, J. Gryboś, Z. Sojka, K. Pacultová, W. Schwieger, A. Volodarskaja, P. Kuśtrowski, A. Rokicińska, D. Fridrichová, L. Obalová, Appl. Catal. B Environ. 255 (2019), 117745, https://doi.org/10.1016/j.apcatb.2019.117745.
[18] Z. Zhang, G. Zhao, W. Li, J. Zhong, J. Xie, Fuel 307 (2022), 121799, https://doi.org/10.1016/j.fuel.2021.121799.
[19] M. Frey, T. Romero, A. Roger, D. Edouard, Catal. Today 273 (2016) 83–90, https://doi.org/10.1016/j.cattod.2016.03.016.
[20] K. Urasaki, S. Kado, A. Kiryu, K. Imagawa, K. Tomishige, R. Horn, O. Korup, Y. Suehiro, Catal. Today 299 (2018) 219–228, https://doi.org/10.1016/j.cattod.2017.06.011.
[21] C. Italiano, R. Balzarotti, A. Vita, S. Latorrata, C. Fabiano, L. Pino, C. Cristiani, Catal. Today 273 (2016) 3–11, https://doi.org/10.1016/j.cattod.2016.01.037.
[22] N.V. Shikina, S.A. Yashnik, A.A. Gavrilova, O.A. Nikolaeva, L.S. Dovlitova, A. V. Ishchenko, Z.R. Ismagilov, Kinet. Catal. 61 (2020) 809–823, https://doi.org/10.1134/S0023158420050110.
[23] G. Grzybek, P. Stelmachowski, P. Indyka, M. Inger, M. Wilk, A. Kotarba, Z. Sojka, Catal. Today 257 (2015) 93–97, https://doi.org/10.1016/j.cattod.2015.02.022.
[24] A. Varma, A.S. Mukasyan, A.S. Rogachev, K.V. Manukyan, Chem. Rev. 116 (2016) 14493–14586, https://doi.org/10.1021/acs.chemrev.6b00279.
[25] S. Specchia, G. Ercolino, S. Karimi, C. Italiano, A. Vita, Int. J. Self Propag. High. Temp. Synth. 26 (2017) 166–186, https://doi.org/10.3103/S1061386217030062.
[26] S. Wójcik, G. Ercolino, M. Gajewska, C.W.M. Quintero, S. Specchia, A. Kotarba, Chem. Eng. J. 377 (2019), 120088, https://doi.org/10.1016/j.cej.2018.10.025.
[27] A. Choya, S. Gudyka, B. de Rivas, J.I. Gutiérrez-Ortiz, A. Kotarba, R. López-Fonseca, Appl. Catal. A Gen. 617 (2021), 118105, https://doi.org/10.1016/j.apcata.2021.118105.
[28] A. Choya, B. de Rivas, J.R. González-Velasco, J.I. Gutiérrez-Ortiz, R. López-Fonseca, Appl. Catal. A Gen. 591 (2020), 117381, https://doi.org/10.1016/j.apcata.2019.117381.
[29] A. Choya, B. de Rivas, J.R. González-Velasco, J.I. Gutiérrez-Ortiz, R. López-Fonseca, Appl. Catal. B Environ. 284 (2021), 119712, https://doi.org/10.1016/j.apcatb.2020.119712.
[30] G. Ercolino, P. Stelmachowski, G. Grzybek, A. Kotarba, S. Specchia, Appl. Catal. B Environ. 206 (2017) 712–725, https://doi.org/10.1016/j.apcatb.2017.01.055.
[31] Y. Wu, L. Luo, W. Liu, React. Kinet. Catal. Lett. 97 (2009) 59–67, https://doi.org/10.1007/s11144-009-0019-z.
[32] A.S. Mukasyan, D.O. Moskovskikh, A.A. Nepapushev, J.M. Pauls, S.I. Roslyakov, J. Eur. Ceram. Soc. 40 (2020) 2512–2526, https://doi.org/10.1016/j.jeurceramsoc.2019.12.028.
[33] S. Hadke, M.T. Kalimila, S. Rathkanthiwar, S. Gour, R. Sonkusare, A. Ballal, Ceram. Int. 41 (2015) 14949–14957, https://doi.org/10.1016/j.materresbull.2021.111238.
[34] H. Fathi, S.M. Masoudpanah, S. Alamolhoda, H. Parnianfar, Ceram. Int. 43 (2017) 7448–7453, https://doi.org/10.1016/j.ceramint.2017.03.017.
[35] R. López-Fonseca, C. Jiménez-González, B. de Rivas, J.I. Gutiérrez-Ortiz, Appl. Catal. A Gen. 437–438 (2012) 53–62, https://doi.org/10.1016/j.apcata.2012.06.014.
[36] J.C. Toniolo, A.S. Takimi, C.P. Bergmann, Mater. Res. Bull. 45 (2010) 672–676, https://doi.org/10.1016/j.materresbull.2010.03.001.
[37] D.D. Tuan, H. Yang, N.N. Huy, E. Kwon, T.C. Khiem, S. You, J. Lee, K.-Y.A. Lin, J. Environ. Chem. Eng. 9 (2021), 105809, https://doi.org/10.1016/j.jece.2021.105809.
[38] C. Zhang, Y. Wang, G. Li, L. Chen, Q. Zhang, D. Wang, X. Li, Z. Wang, Appl. Surf. Sci. 532 (2020), 147320, https://doi.org/10.1016/j.apsusc.2020.147320.
[39] L. Liu, Y. Ou, D. Sun, Chem. Eng. J. 426 (2021), 130063, https://doi.org/10.1016/j.cej.2021.130063.
[40] E. Genty, J. Brunet, C. Poupin, S. Ojala, S. Siffert, R. Cousin, Appl. Catal. B Environ. 247 (2019) 163–172, https://doi.org/10.1016/j.apcatb.2019.01.081.
[41] P. Stefanov, S. Todorova, A. Naydenov, B. Tzaneva, H. Kolev, G. Atanasova, D. Stoyanova, Y. Karakirova, K. Aleksieva, Chem. Eng. J. 266 (2015) 329–338, https://doi.org/10.1016/j.cej.2014.12.099.
[42] R. Murugan, G. Vijayaprasath, G. Ravi, Superlattice. Micro 85 (2015) 321–330, https://doi.org/10.1016/j.spmi.2015.05.041.
[43] R. Dziembaj, A. Chojnacka, Z. Piwowarska, M. Gajewska, M. Swietoslawski, S. Górecka, M. Molenda, Catal. Today 333 (2019) 196–207, https://doi.org/10.1016/j.cattod.2018.03.042.
[44] B. de Rivas, R. López-Fonseca, C. Jiménez-González, J.I. Gutiérrez-Ortiz, J. Catal. 281 (2011) 88–97, https://doi.org/10.1016/j.jcat.2011.04.005.
[45] T. Cai, W. Deng, P. Xu, J. Yuan, Z. Liu, K. Zhao, Q. Tong, D. He, Chem. Eng. J. 395 (2020), 125071, https://doi.org/10.1016/j.cej.2020.125071.
[46] H. Sohn, G. Celik, S. Gunduz, D. Dogu, S. Zhang, J. Shan, F.F. Tao, U.S. Ozkan, Catal. Lett. 147 (2017) 2863–2876, https://doi.org/10.1007/s10562-017-2176-4.
[47] C. Italiano, M.A. Ashraf, L. Pino, C.W.M. Quintero, S. Specchia, A. Vita, Catalysts 8 (2018) 448, https://doi.org/10.3390/catal8100448.
[48] J.R. Paredes, E. Díaz, F.V. Díez, S. Ordóñez, Energ. Fuel. 23 (2009) 86–93, https://doi.org/10.1021/ef800704e.
[49] W. Barrett, S. Nasr, J. Shen, Y. Hu, R.E. Hayes, R.W.J. Scott, N. Semagina, Catal. Sci. Technol. 10 (2020) 4229–4236, https://doi.org/10.1039/D0CY00465K.
[50] A. Choya, B. de Rivas, J.R. González-Velasco, J.I. Gutiérrez-Ortiz, R. López-Fonseca, Appl. Catal. B Environ. 237 (2018) 844–854, https://doi.org/10.1016/j.apcatb.2018.06.050.